Quantifying errors in coral-based ENSO estimates: Toward improved forward modeling of delta O-18

Author:
Stevenson, S.; McGregor, H.V.; Phipps, Steven; Fox-Kemper, B.

Publication details:
Paleoceanography
v. 28
pp. 633-649
1944-9186 (ISSN)

Publication Date:
2013

Publisher DOI:
http://dx.doi.org/10.1002/palo.20059

PALEOCEANOGRAPHY, VOL. 28, 633–649, doi:10.1002/palo.20059, 2013

Quantifying errors in coral-based ENSO estimates: Toward improved forward modeling of $\delta^{18}O$

S. Stevenson,[1] H. V. McGregor,[2] S. J. Phipps,[3] and Baylor Fox-Kemper[4]

Received 28 December 2012; revised 4 September 2013; accepted 6 September 2013; published 16 October 2013.

[1] The oxygen isotopic ratio ($\delta^{18}O$) in tropical Pacific coral skeletons reflects past El Niño–Southern Oscillation (ENSO) variability, but the $\delta^{18}O$-ENSO relationship is poorly quantified. Uncertainties arise when constructing $\delta^{18}O$ data sets, combining records from different sites, and converting between $\delta^{18}O$ and sea surface temperature (SST) and salinity (SSS). Here we use seasonally resolved $\delta^{18}O$ from 1958 to 1985 at 15 tropical Pacific sites to estimate these errors and evaluate possible improvements. Observational uncertainties from Kiritimati, New Caledonia, and Rarotonga are 0.12–0.14‰, leading to errors of 8–25% on the typical $\delta^{18}O$ variance. Multicoral syntheses using five to seven sites capture the principal components (PCs) well, but site selection dramatically influences ENSO spatial structure: Using sites in the eastern Pacific, western Pacific warm pool, and South Pacific Convergence Zone (SPCZ) captures "eastern Pacific-type" variability, while "Central Pacific-type" events are best observed by combining sites in the warm pool and SPCZ. The major obstacle to quantitative ENSO estimation is the $\delta^{18}O$/climate conversion, demonstrated by the large errors on both $\delta^{18}O$ variance and the amplitude of the first principal component resulting from the use of commonly employed bivariate formulae to relate SST and SSS to $\delta^{18}O$. Errors likely arise from either the instrumental data used for pseudoproxy calibration or influences from other processes ($\delta^{18}O$ advection/atmospheric fractionation, etc.). At some sites, modeling seasonal changes to these influences reduces conversion errors by up to 20%. This indicates that understanding of past ENSO dynamics using coral $\delta^{18}O$ could be greatly advanced by improving $\delta^{18}O$ forward models.

Citation: Stevenson, S., H. V. McGregor, S. J. Phipps, and B. Fox-Kemper (2013), Quantifying errors in coral-based ENSO estimates: Toward improved forward modeling of $\delta^{18}O$, *Paleoceanography*, *28*, 633-649, doi:10.1002/palo.20059.

1. Introduction

[2] The El Niño-Southern Oscillation (ENSO) is the dominant source of interannual climate variability and influences atmospheric and oceanic conditions worldwide [*Horel and Wallace*, 1981; *Ropelewski and Halpert*, 1986]. This makes the issue of ENSO's response to future climate change a key question, but to date the scientific community has been unable to provide an answer. Model projections of 21st century ENSO strength disagree widely [*Guilyardi et al.*, 2009], and the disagreement does not seem to be a function of overall model performance [*Collins et al.*, 2010]. Given that large unforced modulations are seen in multicentury simulations [*Wittenberg*, 2009; *Stevenson et al.*, 2010], the disagreement between 21st century ENSO projections created with different Intergovernmental Panel on Climate Change-class climate models may be due in large part to unforced internal variability [*Stevenson et al.*, 2012].

[3] A major roadblock to constraining the ENSO response to climate change is the limited amount of available data on past ENSO variability. The modern instrumental record is too short to detect the climate change signal against the background of natural variability [*Stevenson et al.*, 2010], and most instrumental data are used by modeling centers to "tune" the models during the development process. So even with a longer instrumental record, multimodel projections would still be somewhat suspect, not having the option to test the models against out-of-sample data. To construct independent calibration and verification periods of sufficient length, the only option is to use paleoclimatic proxies to provide information predating the start of the modern record.

[4] The major difficulty with model ENSO validation using proxy evidence is the need for quantitative

Additional supporting information may be found in the online version of this article.

[1]International Pacific Research Center, University of Hawaii at Manoa, Honolulu, Hawaii, USA.
[2]School of Earth and Environmental Sciences, University of Wollongong, Wollongong, New South Wales, Australia.
[3]Climate Change Research Centre and ARC Centre of Excellence for Climate System Science, University of New South Wales, Sydney, New South Wales, Australia.
[4]Department of Geological Sciences, Brown University, Providence, Rhode Island, USA.

Corresponding author: S. Stevenson, International Pacific Research Center, University of Hawaii at Manoa, 1000 Pope Rd., Honolulu, HI 96822, USA. (slgs@hawaii.edu)

0883-8305/13/10.1002/palo.20059

comparisons between proxy data and climate model output, which requires a proxy whose variability depends primarily on ENSO and whose behavior can be well described as a function of its environment. The oxygen isotopic ratio (δ^{18}O) in the aragonite skeletons of tropical corals satisfies both of these requirements, providing seasonally resolved records throughout the tropical Pacific. Coral δ^{18}O has therefore been used successfully to infer past ENSO variability [*Cole et al.*, 1993; *Dunbar et al.*, 1994; *Charles et al.*, 1997; *Evans et al.*, 1998b; *Urban et al.*, 2000; *Tudhope et al.*, 2001; *Cobb et al.*, 2003; *Lough*, 2004; *McGregor and Gagan*, 2004; *Lough*, 2010; *McGregor et al.*, 2011; *Nurhati et al.*, 2011; *McGregor et al.*, 2013]. But obstacles to using coral δ^{18}O to evaluate model performance still remain, arising from our limited understanding of the details of the ENSO influence on δ^{18}O at proxy sites.

[5] Coral δ^{18}O depends primarily on two quantities: SST and the δ^{18}O of seawater. The SST dependence is an inverse relationship, created by thermodynamic fractionation [*Epstein et al.*, 1953] with estimated slopes generally between –0.18 and –0.21‰/°C (see review of *Grottoli and Eakin* [2007]). The δ^{18}O of local seawater is incorporated into the coral skeleton during growth [e.g., *Gagan and Abram*, 2011], which results in a direct proportionality between coral and seawater δ^{18}O; seawater δ^{18}O is then typically represented as proportional to SSS [*LeGrande and Schmidt*, 2006]. Although seawater δ^{18}O is affected by precipitation, evaporation, and advection (see also section 7) [*Fairbanks et al.*, 1997], enhanced rainfall normally leads to more negative δ^{18}O values due to the fact that precipitation tends to be isotopically much more negative than seawater δ^{18}O; thus, more negative coral δ^{18}O values are associated with warm/wet conditions and more positive δ^{18}O values with cold/dry conditions [*Grottoli and Eakin*, 2007]. However, it is possible for the influences of temperature and precipitation on δ^{18}O to partially cancel one another in some locations [*Cahyarini et al.*, 2008]. Other influences, such as small-scale circulations, river runoff, or orographic precipitation, may affect coral δ^{18}O in some locations as well.

[6] The complexity of controls on coral δ^{18}O makes it difficult to convert between model output and the proxy signal, a requirement for quantitative model validation. Statistical methodologies which reconstruct a climatic variable from multiple combined signals [*Evans et al.*, 2002] are sometimes used to overcome this obstacle. However, these methods are limited by the assumption that large-scale climate variability has a stationary structure, as well as by the quality of instrumental data used to calibrate the reconstruction [*Emile-Geay et al.*, 2013]. Thus, empirically derived relationships between coral δ^{18}O and conditions local to each individual site are sometimes also used. In this case, the *local* climate-δ^{18}O relationship is assumed constant, which places a weaker stationarity restriction on large-scale variability. Local conversions either use a "calibration," where proxy data are converted into estimates of observations or model output, or (in the other direction) a "pseudoproxy/forward model" to estimate the proxy signal [*Dunbar et al.*, 1994; *Brown et al.*, 2008; *Thompson et al.*, 2011; *Carré et al.*, 2012; *Smerdon*, 2012; *Phipps et al.*, 2013]. Although the true local relationship may not remain stationary, as the tree ring community has discovered [*D'Arrigo et al.*, 2006], site-specific conversions incorporate the best available knowledge of controls on the proxy signal and have gained popularity recently for estimating past ENSO variability [*Brown et al.*, 2008; *Thompson et al.*, 2011]. However, to date, there has been no systematic quantification of the magnitudes of errors associated with pseudoproxy-based ENSO amplitude estimates—a critical task for determining the extent to which model/proxy disagreement is actually a result of model error.

[7] Here we use modern observations and coral records to evaluate sources of error in coral-based ENSO reconstruction. The conceptual framework is laid out in section 2, data and methods in section 3, issues related to errors in δ^{18}O observations in section 4, and errors in linear pseudoproxies in section 5, including the impact of inaccuracies in observational SST and SSS products. Section 6 then analyzes the degree to which single-site conversions can be improved by including site-specific information. Finally, suggestions for new directions for the paleoclimate community are presented in section 7.

2. Conceptual Framework

[8] In general, a proxy signal P (i.e., the δ^{18}O time series) can be modeled as a function of a set of variables $\mathbf{x}$ (i.e., temperature and/or salinity):

$$P = f(\mathbf{x}) + \epsilon \tag{1}$$

where f represents the relation between P and $\mathbf{x}$, and ϵ is the associated error (e.g., Gaussian white noise).

[9] Paleoclimate calibration/pseudoproxy studies often assume that the proxy signal P is a linear function of just one to two climate variables. Contributions from additional variables may be present as well and may lead to nonlinearities (for instance, advection of water masses carrying distinct δ^{18}O signatures). The goal of quantitative model/proxy comparison is to determine the function f which describes as much of the signal P as possible.

[10] The complexity of potential influences on a proxy signal can be mathematically visualized by applying a Taylor expansion to approximate the function f as a combination of its derivatives, which provides an arbitrarily accurate estimate of f by including more and more terms in the expansion. This is equivalent to deriving higher and higher-order calibration slopes for P as more becomes known about the generation of the signal. For a bivariate expansion, as is generally applied to coral δ^{18}O, f can be estimated near the point $\mathbf{x_0} = (x_0, y_0)$ (where x_0, y_0 represent mean conditions, such as SST and seawater δ^{18}O values) using

$$f(x,y) \approx f(x_0,y_0) + (x-x_0)\frac{\partial f}{\partial x}|_{x_0,y_0} + (y-y_0)\frac{\partial f}{\partial y}|_{x_0,y_0} + \underbrace{(x-x_0)(y-y_0)\frac{\mathrm{d}^2 f}{\mathrm{d}x\mathrm{d}y}|_{x_0,y_0} + \frac{1}{2}(x-x_0)^2\frac{\partial^2 f}{\partial x^2}|_{x_0,y_0} + \frac{1}{2}(y-y_0)^2\frac{\partial^2 f}{\partial y^2}|_{x_0,y_0} + \cdots}_{} \tag{2}$$

[11] The upper line of (2) contains linear dependencies on x and y, and for a bivariate pseudoproxy, the derivatives $\frac{\partial f}{\partial x}|_{x_0,y_0}$ and $\frac{\partial f}{\partial y}|_{x_0,y_0}$ are equivalent to the SST and SSS calibration slopes. The Taylor expansion illustrates that even a bivariate relationship may contain higher-order nonlinear variability (bracketed terms in (2)), although this is typically

Table 1. Modern (Twentieth Century) Coral Sites Used for Monte Carlo Error Estimation[a]

Record	Citation	Time Period	Samples/Year	N3.4/SST	N3.4/SSS	N3.4/δ^{18}O
Clipperton	*Linsley et al.* [1994]	1707–1984	12	0.43	–0.14	–0.38
Kiritimati	Multiple; see *McGregor et al.* [2011]	1938–2007	12	0.74	0.22	–0.51
Laing	*Tudhope et al.* [2001]	1884–1993	4	–0.39	–0.02	0.45
Madang	*Tudhope et al.* [2001]	1880–1993	4	–0.39	–0.05	0.54
Maiana	*Urban et al.* [2000]	1840–1994	6	0.69	0.13	–0.49
New Caledonia	*Stephans et al.* [2004]	1657–1992	4	–0.33	–0.10	0.31
Nauru	*Guilderson and Schrag* [1999]	1891–1995	4	0.60	0.10	–0.43
Palmyra	*Cobb et al.* [2001]	1886–1998	12	0.73	0.005	–0.55
Secas	*Linsley et al.* [1994]	1894–1984	10	0.70	–0.03	–0.25
Tarawa	*Cole et al.* [1993]	1893–1989	12	0.69	0.13	–0.51
Bunaken	*Charles et al.* [2003]	1860–1990	12	–0.09	–0.22	0.44
Savusavu	*Bagnato et al.* [2004]	1940–2001	9	–0.44	0.10	0.64
Vanuatu (Malo Channel)	*Kilbourne et al.* [2004]	1928–1992	12–14	–0.42	0.07	0.60
Vanuatu (Sabine Bank)	*Gorman et al.* [2012]	1842–2007	12	–0.42	0.07	0.53
Rarotonga	*Linsley et al.* [2006]	1726–1999	8	–0.30	–0.15	0.52

[a]The "Samples/Year" entry refers to the sampling resolution of the raw data; "N3.4/SST" and "N3.4/SSS" refer to the correlation coefficient (r) between NINO3.4 SST and SST or SSS closest to the coral location. "N3.4/δ^{18}O" refers to the correlation between coral δ^{18}O and NINO3.4 SST. All correlations are computed using the ERSSTv3b product (SST) or the *Delcroix et al.* [2011] product (SSS). The Kiritimati record is a stacked time series, described in *McGregor et al.* [2011].

neglected. Furthermore, x and y may not completely describe f; other variables might affect δ^{18}O (i.e., advection, runoff).

[12] In paleoclimate applications, data from multiple locations are typically combined to minimize nonclimatic influences. This can be represented mathematically as modifying (1) by an operator B:

$$P = \sum_{i=1}^{N} f(\mathbf{x_i}) \cdot B + \sum_{i=1}^{N} \epsilon_i \cdot B \tag{3}$$

where P is now the combined proxy signal. For instance, to obtain mean δ^{18}O, B becomes an averaging operator. Alternately, to reconstruct NINO3.4 SST [*Emile-Geay et al.*, 2013], B would then become an operator representing the "regularized expectation maximization" algorithm.

[13] The dominant sources of error in model/proxy conversions can be classified as follows:

[14] 1. Nonlinearities in (2): i.e., analytical uncertainty in the proxy signal measurement, feedbacks between variables, or biological influences (section 4.1).

[15] 2. Uncertainty in B: this might arise from temporal nonstationarity (changes to the relationship between variability at the proxy site and the signal of interest), i.e., true changes to the character of El Niño events, apparent changes due to undersampling of internal variability, or shifts in the relation between SSS and seawater δ^{18}O due to changing water mass properties. The choice of sampling locations could also be interpreted as a change in B, where different ENSO signatures appear depending on the network of sites employed (section 4.2).

[16] 3. Errors in observational products: uncertainties in individual in situ measurements, the gridding/interpolation process, or problems with the construction of a reanalysis product (applies only to pseudoproxies derived from gridded climate data; section 5).

[17] 4. Too few or incorrect choices of variables used to constrain $\mathbf{f(x)}$: i.e., not accounting for important processes affecting the coral δ^{18}O signal, such as local river runoff or changes to the δ^{18}O value of precipitation (section 6).

[18] 5. Other local influences affecting the variables $\mathbf{x}$, such as upwelling or local reef circulations: i.e., the action of waves and/or tides, or the interaction of large-scale currents with subsurface island topography (insufficient information to estimate).

[19] Errors of types 1–4 will all contribute to noise ϵ; quantitative estimates of ϵ from various sources are therefore essential. Errors of type 5 cannot be constrained accurately at the moment, and future efforts to assess their influences are recommended.

[20] In this study, δ^{18}O is converted to climate variables via a linear pseudoproxy relationship, where the independent variables are sea surface temperature and salinity (proportional to seawater δ^{18}O):

$$\mathbf{P} = \beta_0 + \beta_T(\mathrm{SST}) + \beta_S(\mathrm{SSS}) + \epsilon_{\mathrm{lin}} \tag{4}$$

Here ϵ_{lin} refers to the uncertainties associated with the linear relationship.

[21] Equation (4) follows previously adopted linear relationships [*Thompson et al.*, 2011]. Its limitations are discussed in section 5, and potential improvements are then presented in sections 6 and 7.

3. Data and Methods

[22] Modern δ^{18}O records are selected from the World Data Center for Paleoclimatology (WDCP) in the tropical Pacific (23°S–23°N), and all records are included for which the following criteria are met:

[23] 1. Temporal resolution of ≥4 measurements/yr (seasonal),

[24] 2. Correlation between coral δ^{18}O and SST in the NINO3.4 region (5°S–5°N, 170–120°W) significant at or above the 90% confidence level.

[25] This leads to the selection of 15 proxy sites (Table 1). At some locations multiple records are available: two coral records were collected at Nauru [*Guilderson and Schrag*, 1999] and at Savusavu [*Bagnato et al.*, 2004], three at New Caledonia [*Stephans et al.*, 2004] and Rarotonga [*Linsley et al.*, 2006], and six at Kiritimati [*Evans et al.*, 1998a; *Woodroffe and Gagan*, 2000; *Woodroffe et al.*, 2003; *Nurhati et al.*, 2009; *McGregor et al.*, 2011]. For Kiritimati, the published stack of *McGregor et al.* [2011] is used except where otherwise indicated. For other sites,

Table 2. Kiritimati Island Coral Records Used to Estimate Errors Due To δ^{18}O Signal/Dating Uncertainties

Record	Citation	Time Period
Evans 1	*Evans et al.* [1998a]	1938–1993
Evans 2	*Evans et al.* [1998a]	1981–1986
Nurhati	*Nurhati et al.* [2009]	1972–1998
McGregor	*McGregor et al.* [2011]	1994–2007
Woodroffe 1	*Woodroffe and Gagan* [2000]	1978–1991
Woodroffe 2	*Woodroffe et al.* [2003]	1989–1999

a single core has been chosen to represent each location (core "92 PAA" from New Caledonia [*Quinn et al.*, 1998], core "3R" from Rarotonga [*Linsley et al.*, 2006], and core "LH" at Savusavu [*Bagnato et al.*, 2004]; our tests showed that results are insensitive to the choice of coral for a given site). Variations within a single site (section 4.1) are estimated using the records listed in Table 1 from New Caledonia and Rarotonga, as well as the six short δ^{18}O records from Kiritimati Island used to construct the stacked Kiritimati time series (Table 2). For the network analysis of section 4.2 and the pseudoproxy calculations of section 5, the time period 1958–1990 is used to maximize simultaneous data availability.

[26] Unless otherwise specified, all SST data are taken from the NOAA Extended Reconstructed SST product (ERSSTv3b) [*Smith et al.*, 2008] and all SSS data are taken from the ship-of-opportunity database constructed by *Delcroix et al.* [2011], since these products both supply grid point standard deviations. Grid points for SST and SSS data are chosen from the four nearest neighbors for each proxy site, such that the correlation with δ^{18}O is maximized. A complete accounting of the grid points selected for each site and data product is provided in the supporting information.

[27] SST and SSS data were linearly interpolated to match the calendar dates associated with the coral age models. Table 1 provides correlation coefficients between NINO3.4 and grid point SST and SSS. For most sites the correlation with SST is above 0.4, and for some locations (e.g., Nauru and Tarawa) the correlation with SSS is substantial as well (see correlation maps in Figure S1). This demonstrates the feasibility of coral-based ENSO amplitude reconstructions from these sites (see section 4.2).

4. Observational Constraints

[28] Errors in the coral observations themselves are first examined, by separately considering issues arising from combining multiple measurements at a single site (section 4.1) and from constructing an ENSO amplitude estimate from multiple δ^{18}O time series (section 4.2).

4.1. Signal/Age Model Errors

[29] Owing to the difficulty of collecting contemporaneous fossil corals from multiple locations, many coral paleoclimate studies rely on a single δ^{18}O time series from each site. Thus, replication studies often compute estimates from present-day corals and assume that similar errors are present in fossil corals. Here an error analysis for modern corals is performed at the three tropical Pacific sites for which at least three simultaneous, seasonally resolved δ^{18}O time series were available: Amedee Lighthouse in New Caledonia (22.5°S, 166.5°E) [*Stephans et al.*, 2004], Rarotonga (21.2°S, 159.8°E) [*Linsley et al.*, 2006], and Kiritimati Island (2°N, 157°W; Table 2).

[30] If the analytical δ^{18}O measurement error is ignored, the dominant uncertainties in single-site δ^{18}O variance are here referred to as the "signal" and "age model" errors; the δ^{18}O time series contain a combination of both. Signal error consists of local (external) or biological (internal) processes unrelated to large-scale climate. External signal errors likely arise from small-scale climate influences near the reef [*McGregor et al.*, 2011], or other factors acting on the coral (i.e., fish bites) [*Linsley et al.*, 1999]. Internal signal errors might arise from coral vital effects (i.e., the "spawning spikes" of *Evans et al.* [1999]), growth rate influences [*Gagan et al.*, 2012], or diagenesis [*McGregor and Abram*, 2008].

[31] Age model error is generated during the process of assigning calendar months to δ^{18}O measurements within a given year [*Evans et al.*, 1999; *Felis et al.*, 2000; *Cobb et al.*, 2003] and is well constrained in comparison to signal error. Age model construction is typically done by assigning at least one fixed "tie point" per year and interpolating between the tie points. Tie points may be assigned to the annual coldest month (maximum δ^{18}O) or warmest month (minimum δ^{18}O) [*Linsley et al.*, 1994; *Felis et al.*, 2000; *Cobb et al.*, 2003]. Sr/Ca measurements are sometimes used for assigning times [*DeLong et al.*, 2007], as are coral δ^{13}C [*Cole et al.*, 1993; *Evans et al.*, 1999; *Guilderson and Schrag*, 1999; *Tudhope et al.*, 2001]. During an El Niño year when the δ^{18}O seasonal cycle is suppressed, either a constant growth rate is assumed or the density band structure is used (where available, e.g., *Linsley et al.* [1994], *Quinn et al.* [1998], *Tudhope et al.* [2001], *Cobb et al.* [2003], and *McGregor et al.* [2011], among others). Season matching against instrumental data can then provide additional accuracy [*Gagan et al.*, 1998].

[32] To combine records from a given site, the δ^{18}O values for each record are adjusted by adopting a single δ^{18}O time series as the "reference" and offsetting the others such that the means of the overlapping portions are identical. The time series of each individual δ^{18}O record (after adjustment) is then shown in Figure 1, for the 1975–2005 period. The standard deviation σ measures signal and age model errors combined; this was computed by taking the variance as a function of time, for each month having $\geq$ two measurements, then computing the square root of the mean variance. The mean σ is 0.14‰ at Kiritimati, 0.14‰ at New Caledonia, and 0.12‰ at Rarotonga. The agreement in signal/age model error estimates between sites is remarkable and suggests that this result is quite robust. Notably, this error is of the same order of magnitude as the analytical uncertainty (0.05–0.08‰); perhaps, the signal error is due in large part to the δ^{18}O measurements themselves, or to sampling errors introduced during the construction of the δ^{18}O time series [*Alibert and Kinsley*, 2008; *McGregor et al.*, 2011; *DeLong et al.*, 2013].

[33] The remaining portion of the signal error most likely reflects the effects either of local circulation in the reef environment (generally minimized at the time of collection) or of other biological factors. Here both "head" and "microatoll" forms of the *Porites* species from Kiritimati are included (Table 2); microatolls tend to grow in much

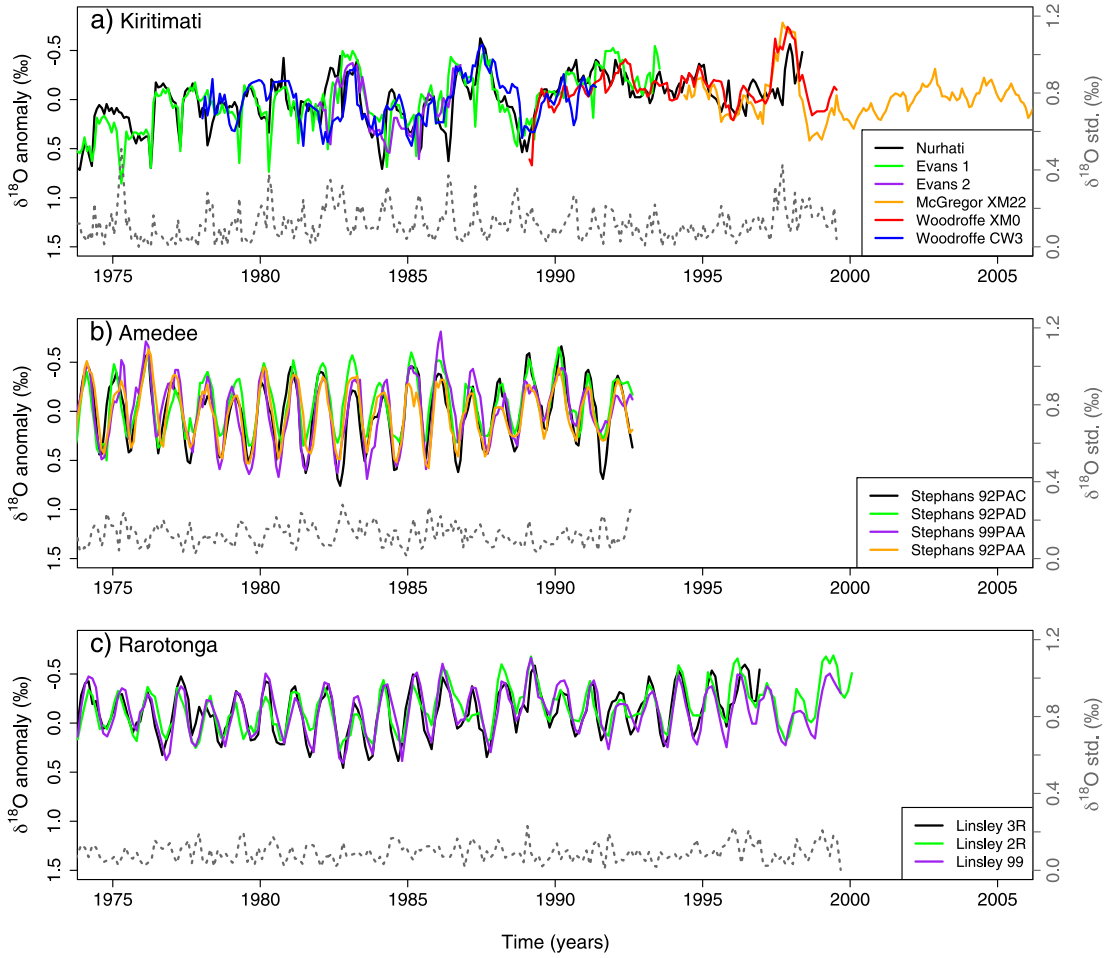

Figure 1. Stacked δ^{18}O anomaly time series (‰; note reversal of the *y* axis). Colored lines represent different δ^{18}O records, referenced to a particular coral (thick black line) such that overlapping means are identical. Gray dotted lines indicate the standard deviation between all coral records as a function of time (‰). (a) Kiritimati; month-long excursions observed in the *Evans et al.* [1998b] record (Evans 1) are due to spawning spikes. All corals have been referenced to the *Nurhati et al.* [2011] data set (blue), which results in offsets of 0.19‰ (Evans 1), 0.12‰ (Evans 2), –0.25‰ (McGregor XM22), –0.27‰ (Woodroffe XM0), and –0.22‰ (Woodroffe CW3). (b) Amedee; all data from *Stephans et al.* [2004]. Reference coral is the "92 PAC" sample, resulting in offsets of –0.1‰ (92 PAD), –0.02‰ (99 PAA), and –0.16‰ (92 PAA). (c) Rarotonga; all data taken from *Linsley et al.* [2006]. Reference coral is the "3R" sample, resulting in offsets of 0.10‰ (2R) and –0.08‰ (99). In all panels, a positive offset indicates that a time series has a lighter (less negative) mean δ^{18}O value than the reference.

shallower water than head corals but are as sensitive as head corals to large-scale ocean conditions [*McGregor et al.*, 2011]. The error estimates here are largely unaffected by exclusion of the microatoll corals from analysis (not pictured), suggesting that other effects, such as "spawning spikes" [*Evans et al.*, 1999] or diagenesis [*Nurhati et al.*, 2011; *LaVigne et al.*, 2013], dominate. In addition, the Kiritimati δ^{18}O records derive from all *Porites* growth forms, growing at different rates on different parts of the island, and have been analyzed at three different labs; the analyses are therefore quite independent. Although produced by a single team in each case, which might be expected to result in a slight reduction of error relative to Kiritimati, the Amedee and Rarotonga sites provide further verification of the Kiritimati estimates. Thus, the 0.12–0.14‰ value can be considered a reasonable first-order approximation of signal/age model uncertainties. A full attribution of sources of error would require a comprehensive comparison with in situ seawater δ^{18}O measurements, which is not possible at present.

[34] We next consider the implications of intrasite δ^{18}O offsets for the error on the "true" δ^{18}O variance. For Kiritimati, Amedee, and Rarotonga, the site-specific signal/age model error is used; elsewhere, the mean of those three sites is adopted. The signal/age model error value is used as the uncertainty on each individual measurement, which is added as Gaussian noise to the δ^{18}O time series to compute Monte Carlo samples (see section 5 for methods). The standard error is then calculated by taking the standard deviation of the Monte Carlo δ^{18}O variances, which results in a range of

Table 3. Variance of δ^{18}O From the Modern Samples, a Comparison of That Variance With Signal/Age Model Influences Expressed as a Percentage ($\sigma^2_{age}/\sigma^2_{\delta^{18}O} \times 100\%$), and the Associated Standard Error on the Variance Resulting From Propagation of the Signal/Age Model Error (Σ_{age})[a]

Coral	σ^2 δ^{18}O (‰^{2})	σ^2_{age}/σ^2 δ^{18}O (%)	Σ_{age} (‰^{2})	Σ_{age} (%)
Bunaken	0.030	63	0.0046	16
Clipperton	0.016	119	0.0040	25
Kiritimati	0.077	25	0.0068	10
Laing	0.026	73	0.0043	18
Madang	0.031	61	0.0044	16
Maiana	0.060	32	0.0058	11
Nauru	0.070	27	0.0068	10
New Caledonia (Amedee)	0.065	30	0.0074	11
Palmyra	0.036	53	0.0050	14
Rarotonga	0.037	39	0.0041	12
Savusavu	0.044	43	0.0051	13
Secas	0.130	15	0.0090	8
Tarawa	0.036	53	0.0046	14
Vanuatu (Malo Channel)	0.048	40	0.0053	12
Vanuatu (Sabine Bank)	0.039	49	0.0051	13

[a]For Kiritimati, Amedee, and Rarotonga, the signal/age model error for that site is used (σ_{age} = 0.14, 0.14 and 0.12‰, respectively). For all other sites, the mean of the three signal/age model error estimates is applied.

8–25% depending on the site (Table 3). This range approximates (but is not necessarily identical to) the true signal/age model errors, in the absence of a full replication analysis at other locations.

4.2. Multiple Site Combination

[35] Combining the δ^{18}O signal from multiple locations is often used to help mitigate local uncertainties; this is equivalent to applying the combination operator B in (3). A common choice of B is the first principal component, or PC1, as this captures the dominant covarying signal across sites. For the coral sites in Table 1, the relationship between PC1 of coral δ^{18}O and ENSO is verified in Figure 2. The PC1 time series has a correlation coefficient of –0.62 with NINO3.4 SST, much stronger than the correlation between NINO3.4 and any other δ^{18}O principal component (not pictured). Therefore, PC1 is presumed to contain the largest proportion of ENSO-related variability.

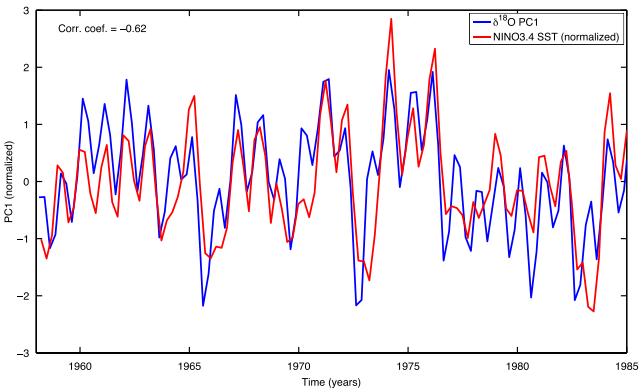

Figure 2. Verification that coral δ^{18}O PC1 contains ENSO-related variability; here PC1 is derived from the coral δ^{18}O records listed in Table 1. Time series of the coral PC1 (blue) is compared with NINO3.4 SST (red) from HadISST [*Rayner et al.*, 2003]). Both time series have been normalized to have zero mean and unit standard deviation.

[36] First, the contribution of signal/age model errors (Section 4.1) to uncertainties on PC1 is considered. This is done by drawing values randomly from a Gaussian PDF with zero mean and a standard deviation equal to the signal/age model error, then adding them to the input δ^{18}O time series for each Monte Carlo sample; the PC1 is then recalculated. The red envelope in Figure 3a shows the resulting scatter in the PC1 power spectrum, and the major spectral features in δ^{18}O PC1 remain clearly identifiable.

[37] Next, dating uncertainties are considered; these are negligible for modern (living) corals which can be compared directly with observations [*Evans et al.*, 1999], but can become large for corals which are dead when collected (for example, in situ fossil corals or storm-washed coral boulders). Unbroken fossil corals overlapping with observations can be dated as accurately as living corals, given additional constraints (e.g., U-Th dating). However, any gaps within a given core will create dating uncertainties which increase

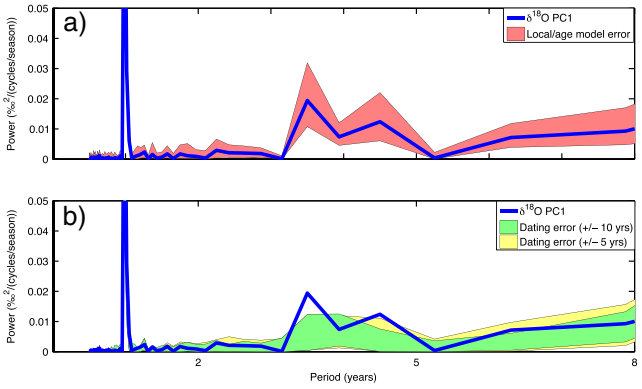

Figure 3. Errors in coral δ^{18}O. The power spectrum of δ^{18}O PC1 derived from modern δ^{18}O records is shown as the blue solid line. Errors from (a) signal/age model effects (red) and (b) dating uncertainties (yellow and green) are shown as envelopes around the coral δ^{18}O PC1. In both the signal/age model and dating uncertainty cases, the major spectral features in δ^{18}O PC1 are still clearly identifiable.

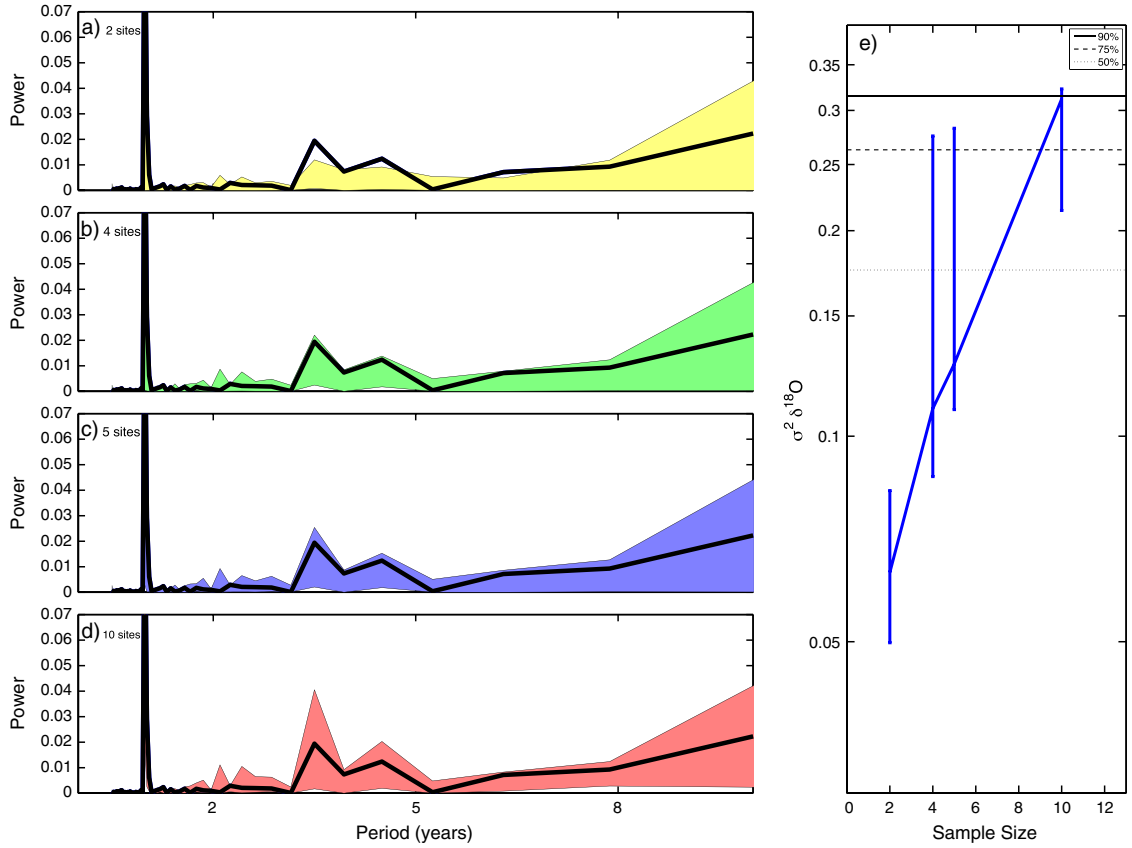

Figure 4. Errors in coral δ^{18}O due to sample size limitations. The power spectrum of PC1 for coral δ^{18}O is shown in black. Shading then indicates δ^{18}O PC1 calculated using varying numbers of randomly selected sites: (a) 2 sites, (b) 4 sites, (c) 5 sites, and (d) 10 sites. The subsample ranges were calculated by selecting a random sample (without replacement) from the full set of corals from Table 1 and then repeating the calculation 100 times. No additional errors are modeled here. (e) Interquartile (25th–75th percentile) range on total variance in δ^{18}O PC1 using the same samples from Figures 4a–4d. Horizontal lines are drawn at 50%, 75%, and 90% of the original δ^{18}O PC1 variance. The majority of the variance in δ^{18}O PC1 is retained when the sample consists of five or more corals; note that only with 10 or more sites does the range include the 2–5 year interannual peak in PC1.

with time [*DeLong et al.*, 2012; *Alibert and Kinsley*, 2008]. In such cases, as well as for cores which do not overlap with observations, radiometric dating must be used to estimate the absolute age of the coral. For the past decade, errors of ±1% [*Cobb et al.*, 2003] have been achievable for high-resolution U/Th dating of "young" fossil corals, which leads to uncertainties of 5–10 years [*Zhao et al.*, 2009]. However, new approaches are able to achieve smaller errors [*Shen et al.*, 2008; *Cheng et al.*, 2013].

[38] Here temporal offsets representing "typical" dating errors are applied to each δ^{18}O time series according to a uniform distribution prior to performing the principal component analysis. Two values are used: 5 years, appropriate for young corals from the past few centuries, and 10 years, appropriate for older corals (i.e., mid-Holocene samples) [*McGregor et al.*, 2013]. The result is shown in Figure 3b and is relatively small, an encouraging indication for future reconstruction efforts. Note that a reduction in the mean interannual variance does occur (on the order of 11%), but since not all simulated time series are offset by the maximum dating error, the majority of variance is retained. The variance reduction is larger for a 10 year error, an average of 14% less than the input δ^{18}O PC1 variance, but the major spectral features remain clearly visible.

[39] The number of sites used to reconstruct ENSO is also important, as using only a few locations will underestimate the amplitude of the basin-scale signal. Coral proxy network construction was studied in detail by *Evans et al.* [1998b], who found that central and eastern Pacific sites added the most skill and that the first six to seven sites achieved half of the total error reduction. A later study by *Evans et al.* [2000] further illustrated that the covarying δ^{18}O modes do represent both ENSO and the twentieth century global warming trend. But there has been relatively little analysis of how the amplitude and character of the covarying δ^{18}O signal is reproduced using small subsamples of tropical Pacific locations, as may be the case for fossil coral applications. To that end, Figures 4a–4d show PC1 spectra for samples of varying sizes drawn from the set of tropical sites. The power in δ^{18}O PC1 is systematically underestimated, but the accuracy increases rapidly with sample size. Using four to five corals captures roughly 30–40% of the total PC1 variability and

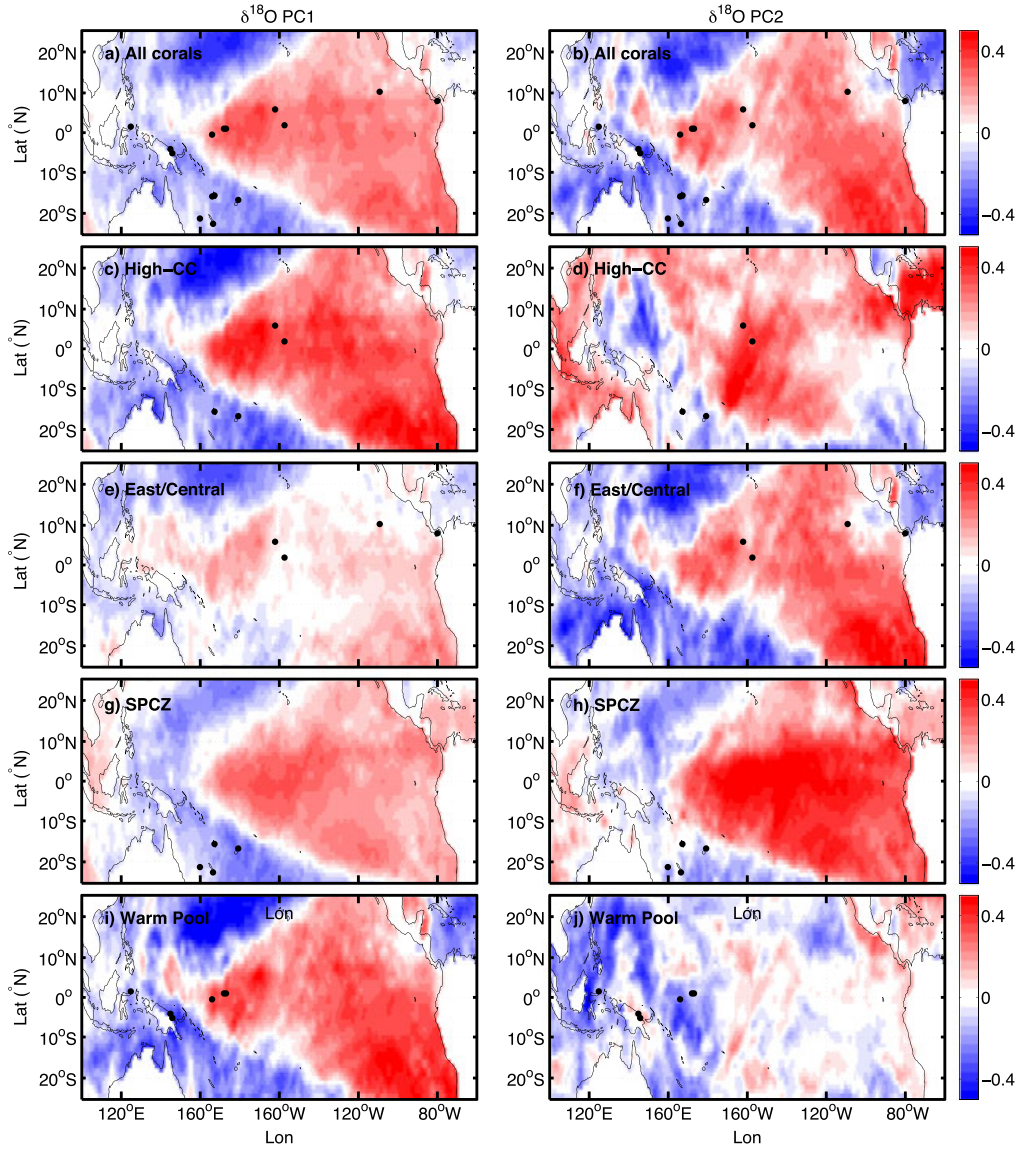

Figure 5. Effect of coral network choice on character of reconstructed ENSO. The SST anomaly from the HadISST data set is correlated with δ^{18}O PCs computed using (a, b) the full set of 17 coral sites listed in Table 1, (c, d) the High CC sample, (e, f) the East/Central sample, (g, h) the SPCZ sample, and (i, j) the Warm Pool sample. Left column indicates correlation between SSTA and coral δ^{18}O PC1 and right column with PC2. In all panels, black circles indicate the position of the sites included in the relevant coral δ^{18}O sample. Most network choices detect eastern Pacific-type El Niño patterns in both δ^{18}O PC1 and PC2; combining the Warm Pool and SPCZ sites (i.e., the High-CC sample) then results in a more Central Pacific-like pattern in δ^{18}O PC2.

90–100% is captured when 9–10 of the 11 corals are retained in the subsample (Figure 4e).

[40] To illustrate the effect of site selection on the *character* of the reconstructed ENSO, the locations in Table 1 are split into several categories:

[41] 1. **High CC**: high correlation between NINO3.4 SSTA and δ^{18}O (here "CC" refers to "correlation coefficient"). This sample includes Savusavu, Palmyra, Kiritimati, and Vanuatu (Malo Channel).

[42] 2. **East/Central**: directly influenced by the equatorial cold tongue in the eastern/central Pacific. This sample includes Clipperton, Secas, Palmyra, and Kiritimati.

[43] 3. **SPCZ**: locations directly influenced by the South Pacific Convergence Zone. This sample includes Vanuatu (both sites), Savusavu, New Caledonia, and Rarotonga.

[44] 4. **Warm Pool**: locations in the western Pacific warm pool. This sample includes Tarawa, Maiana, Laing, Madang, Nauru, and Bunaken.

[45] The PC1 of δ^{18}O from each sample is correlated with basin-wide SST anomaly from HadISST [*Rayner et al.*, 2003] and shown in Figure 5 (left column). The canonical El Niño "horseshoe" is detected by the Warm Pool, SPCZ, East/Central, and High CC samples and is relatively insensitive to sample size (not shown). Thus, reconstruction of

eastern Pacific-type El Niño events seems feasible given four to five δ^{18}O records.

[46] The correlation of SSTA with PC2 of δ^{18}O is shown in Figure 5 (right column). Most samples show a correlation structure resembling PC1, indicating that eastern Pacific El Niño-like variability may be split between δ^{18}O PC modes. But remarkably, in the High CC case (Figure 5d), a distinctive pattern resembling the "El Niño Modoki" of *Ashok et al.* [2007] appears. The central Pacific sites Palmyra and Kiritimati appear in both the High CC and East/Central samples; the greater sensitivity of the High CC sample to "Modoki-like" ENSO variability thus likely derives from the SPCZ-influenced sites Savusavu and Vanuatu. The SPCZ migrates substantially during "Modoki-type" events, and the associated salinity anomalies are extremely large near Savusavu and Vanuatu [*Singh et al.*, 2011]. In contrast, Modoki-like salinity signals at Palmyra are quite weak, which is thought to be a consequence of anomalous mixing due to enhanced wind stress [*Nurhati et al.*, 2011]. Although the present analysis does not allow attribution of the temperature versus salinity-driven portions of δ^{18}O variability, we hypothesize that such differences in salinity sensitivities could be responsible for the ability of the High CC sample to effectively identify ENSO variability centered near the dateline.

[47] These results indicate that effective reconstruction of the complete continuum of "canonical" to Modoki-like ENSO variability [*Ray and Giese*, 2012] requires a combination of records from both the central equatorial Pacific and other locations. An important caveat here is that only a limited subset of locations was used; extending this analysis to include additional sites will provide an improved understanding of the effects of sample construction.

5. Linear Pseudoproxies

[48] Excluding observational considerations, the most important factor in paleo-ENSO reconstruction is the conversion between δ^{18}O and climate variables (e.g., SST and SSS). There is a wealth of literature on calibrating proxy data against local climate (see the review by *Grottoli and Eakin* [2007]), and for coral δ^{18}O, the temperature fractionation effect [*Epstein et al.*, 1953] and dependence on seawater δ^{18}O [*Fairbanks et al.*, 1997; *LeGrande and Schmidt*, 2006] have been studied in detail. What is still missing is a detailed examination of the degree to which uncertainties in climate calibrations introduce errors in forward-modeled proxy signals. The pseudoproxy calculations here are therefore designed to maximize the application of existing knowledge of the controls on coral δ^{18}O, while still providing for the minimization of errors in bivariate linear pseudoproxies of the type adopted by *Brown et al.* [2008] and *Thompson et al.* [2011].

5.1. Pseudoproxy Formulation

[49] The δ^{18}O temperature dependence has been extensively examined in the literature [*Epstein et al.*, 1953; *Correge*, 2006]. Likewise, the relationship of seawater δ^{18}O with salinity has been previously studied [*Fairbanks et al.*, 1997], and basin-scale calibrations derived for all world oceans [*LeGrande and Schmidt*, 2006]. We first take advantage of these existing calibration studies, by applying specified regression coefficients to instrumental SST and SSS in (4), hereafter the "fixed-slope pseudo-δ^{18}O." This is the approach used by *Thompson et al.* [2011] and represents the best available knowledge of the temperature and salinity sensitivities of δ^{18}O.

[50] The δ^{18}O/SST and δ^{18}O/SSS calibration slopes vary significantly from site to site (e.g., *Correge* [2006], for δ^{18}O/SST). Here we adopt a δ^{18}O/SST sensitivity of -0.18 ± 0.04‰/°C, where the –0.18‰/°C coefficient represents the best estimate from the multicoral synthesis of *Gagan et al.* [2012] and the 0.04‰/°C uncertainty reflects an average spread due to growth rate influences. This allows the calibration slope range to include the –0.21‰/°C slope sometimes adopted by other multisite analyses [*Grottoli and Eakin*, 2007].

[51] The errors on our δ^{18}O/SSS slope are larger than those used in the *Thompson et al.* [2011] study, since seawater δ^{18}O measurements are derived from extremely sparse measurements of salinity and seawater δ^{18}O, which may in turn reflect possible nonlinear effects from precipitation/evaporation and oceanic advection (see sections 6 and 7). The *LeGrande and Schmidt* [2006] data set derives δ^{18}O/SSS slopes of 0.27 and 0.45‰/practical salinity unit (psu) for the tropical and South Pacific, respectively. In the absence of a well-constrained site-specific δ^{18}O/SSS slope, the value for any given Pacific location may therefore be expected to lie somewhere between these values. To best approximate the true sensitivity range, a value of 0.36 ± 0.09‰/psu is adopted.

[52] Although the fixed-slope pseudo-δ^{18}O calculation is "optimal" in the sense that it most strongly leverages known SST and SSS calibration data, this approach will not necessarily provide the most accurate climate/δ^{18}O conversions on a site-by-site basis. A smaller uncertainty can be achieved by deriving site-specific relationships using least squares error minimization; this approach will give a smaller overall δ^{18}O error than the fixed-slope method. For comparison, therefore, the δ^{18}O values determined by individual fits of (4) to each δ^{18}O time series are performed and are referred to as the "best fit pseudo-δ^{18}O" time series. The best fit coefficients are calculated using a stepwise linear regression algorithm [*Venables and Ripley*, 2002] and are presented in Table 4. The best fit approach can be considered to give the linear pseudoproxy approximation the "best chance," so to speak, of capturing ENSO amplitude accurately. If even the linear relationship chosen to maximize the δ^{18}O variance explained still cannot provide an accurate prediction of that variance (as section 5.2 will demonstrate), then this is strong evidence that the relationship in (4) is insufficient for accurate δ^{18}O/climate conversion.

5.2. Pseudoproxy Error Estimation

[53] For both the fixed-slope and best fit pseudo-δ^{18}O, errors are estimated using a Monte Carlo approach. The observational uncertainties are computed by sampling from a Gaussian distribution with the appropriate signal/age model error: For sites with only a single core, the average error from the Kiritimati, New Caledonia, and Rarotonga analyses is used, and elsewhere, the measured errors are applied. Uncertainties in SST and SSS are computed based on the error estimates supplied with the ERSSTv3b and *Delcroix et al.* [2011] products, respectively. Errors in δ^{18}O, SST, and SSS are all added prior to the linear fit.

Table 4. Fit Statistics for Conversion From Climate Variables to $\delta^{18}O$[a]

Record	β_0 (‰)	β_T (°C/‰)	β_S (psu/‰)	R^2 (Adjusted)
Bunaken	–6.83	–0.24	–	0.13
Clipperton	–10.2	–0.21	+0.31	0.33
Kiritimati	–14.1	–0.14	–	0.23
Laing	–2.58	–0.32	+0.20	0.37
Madang	–2.32	–0.28	–	0.22
Maiana	–12.4	–0.19	+0.38	0.50
Nauru	–4.07	–0.34	+0.26	0.47
New Caledonia	–13.7	–0.12	+0.35	0.32
Palmyra	+3.20	–0.29	–	0.65
Rarotonga	–15.4	–0.07	+0.36	0.29
Savusavu	–14.7	–0.10	+0.36	0.51
Secas	–9.23	–0.25	+0.32	0.33
Tarawa	–10.8	–0.13	+0.27	0.37
Vanuatu (Malo Channel)	–18.1	–0.12	+0.47	0.58
Vanuatu (Sabine Bank)	–18.9	–0.11	+0.49	0.67

[a]Fit parameters listed are the result of a stepwise regression of $\delta^{18}O$ on SST and SSS (see equation (4) in the main text); the adjusted R^2 is listed in the last column, being a modified form of the coefficient of determination which penalizes fits containing additional independent variables. En dashes (–) indicate that a variable was not included in the best fit regression.

[54] Fits are computed for each biased Monte Carlo sample, and the associated residual errors computed for each location individually. We allow the slope to vary: In the fixed-slope case, the slopes β_T and β_S follow a normal distribution with standard deviation equal to the adopted error for the SST and SSS slopes ($0.04‰/°C$ and 0.09‰/psu respectively). In the best fit case, the slopes are randomized according to the standard errors on β_T and β_S returned from the least squares algorithm. This approach may perhaps underestimate the magnitude of fit errors relative to more sophisticated "errors in variables" algorithms [*Mann et al.*, 2008], but given that errors in the slope do not contribute substantially to the overall uncertainty (not pictured), this should not greatly impact the result.

[55] For each Monte Carlo sample, since the associated best fit intercept (β_0') will change, the regression intercepts for each location are recalculated based on the randomly

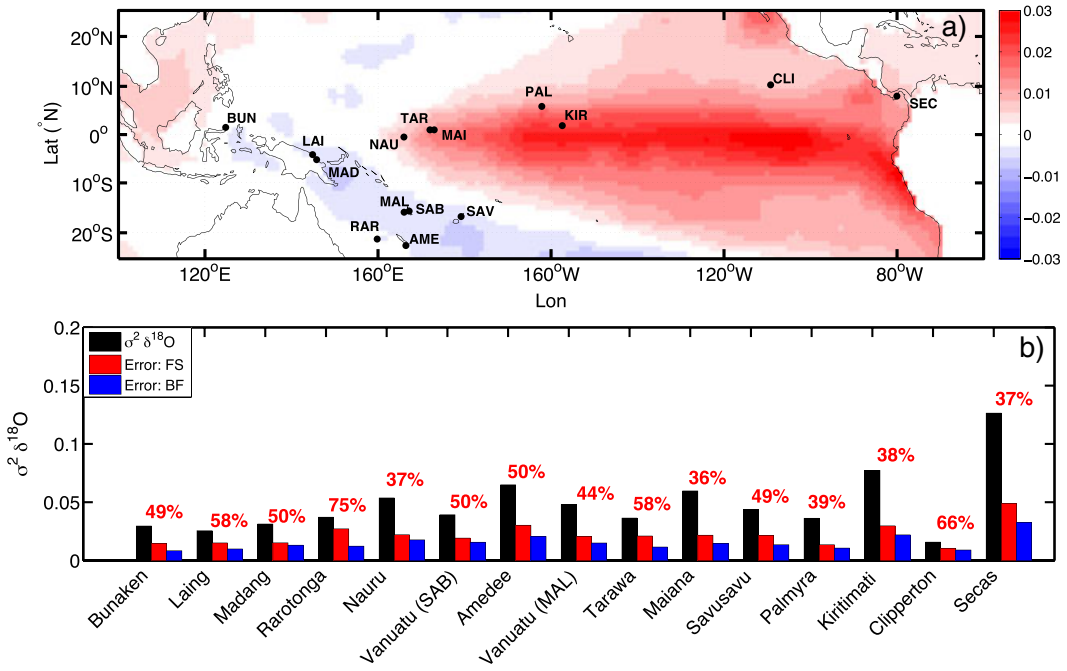

Figure 6. The $\delta^{18}O$ variance error analysis for linear pseudoproxies. (a) Locations of coral sites used in this analysis. Background colors correspond to the spatial pattern of the HadSST EOF1 (dimensionless). (b) Errors on the $\delta^{18}O$ variance for each site. The total $\delta^{18}O$ variance for the 1958–1985 period is shown in black. Errors computed as described in the text using the fixed-slope pseudoproxies are shown in red, and those computed using best fit pseudoproxies are shown in blue. Percentage values listed in red correspond to the errors for the fixed-slope method (shown also in Table 6). The abbreviations "SAB" and "MAL" for the Vanuatu samples refer to the Sabine Bank and Malo Channel sites, respectively (see Table 1).

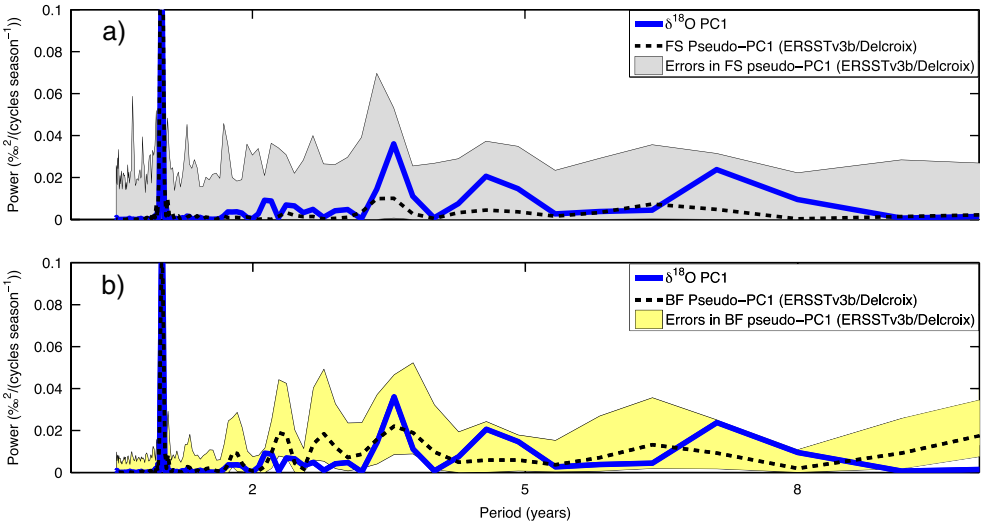

Figure 7. The δ^{18}O PC1 power spectrum error analysis for linear pseudoproxies. (a) PC1 of fixed-slope (FS) pseudo-δ^{18}O. (b) PC1 of best fit pseudo-δ^{18}O. In both panels, pseudo-δ^{18}O PC1 generated from applying equation (4) to observed SST and SSS is shown as the black dashed line. Monte Carlo errors then appear as the shaded envelopes in gray (fixed-slope) or light yellow (best fit). The spectrum for the true δ^{18}O PC1 is shown as the blue solid line. Spectral errors are large in both cases, though slightly smaller for the best fit pseudoproxy.

generated slopes β'_T and β'_S by minimizing the least squares equation:

$$\beta_0 = \frac{1}{N}\left(\sum_{i=1}^{N}\delta^{18}O_i - \sum_{i=1}^{N}\beta'_T T_i - \sum_{i=1}^{N}\beta'_S S_i\right) \quad (5)$$

where N is the number of observations and δ^{18}O, T, and S are the values obtained after applying observational uncertainties. Biased pseudo-δ^{18}O time series are then constructed by adding the pseudo-δ^{18}O values predicted from (5) to an error time series drawn from the probability density function of the fit residuals. The variance of each simulated time series is then computed, and the standard deviation of the simulated variances adopted as the error on the δ^{18}O variance.

[56] Errors in pseudo-δ^{18}O variance are reported in Figure 6b for the fixed-slope and best fit cases. These errors are quite large, ranging roughly from 37 to 75% of the original δ^{18}O variance. The magnitude of the errors indicates that the corresponding ENSO amplitude estimates from linear pseudoproxies will also be highly uncertain, despite the large correlations between δ^{18}O and ENSO [*Brown et al.*, 2008; *Thompson et al.*, 2011]. Combining multiple δ^{18}O signals using PC1 is next performed, in an effort to mitigate the errors depicted in Figure 6; errors on δ^{18}O PC1 calculated from the Monte Carlo δ^{18}O time series are given in Figure 7. As for the single-site pseudo-δ^{18}O variances, computing PC1 does not provide an accurate estimate of the total degree of variability. The pseudo-δ^{18}O PC1 underestimates the magnitude of the peak in δ^{18}O PC1 near 3.5 years, although the peak can still be visually identified. But the large errors in δ^{18}O PC1 indicate that there are systematic errors associated with the pseudoproxy conversion which prevent averaging from eliminating errors in multisite ENSO amplitude estimation. Accounting for the conversion errors appropriately is the reason why the errors in Figure 6 are so much larger than previous error estimates in coral δ^{18}O-based ENSO amplitude [*Hereid et al.*, 2013].

[57] The large errors shown in Figure 6 may result from the observational δ^{18}O errors discussed in section 4. However, there is still the possibility that gridded SST and SSS products do not provide sufficiently accurate information to reconstruct the coral δ^{18}O signal, either because of inaccuracies in the SST or SSS measurements or because of subgrid-scale influences on SST and/or SSS. A good example of the profound implications of differences between observational products is the contrast between two recent studies: *Solomon and Newman* [2012], who removed the ENSO signal from twentieth century data and concluded that there was no trend in the residual Walker circulation, and *Tokinaga et al.* [2012], who showed that a twentieth century weakening of the Walker circulation could be masked by biases in surface wind data sets. Similarly, twentieth century Pacific SST trends were shown by *Deser et al.* [2010] to differ between data products, not only in magnitude but also in sign; the controversies over the twentieth century instrumental record clearly have yet to be resolved.

[58] A rough idea of the contribution of SST and SSS uncertainties to δ^{18}O conversion errors may be gained by examining the effects of differences between observational SST and SSS products on the resulting pseudo-δ^{18}O. This is calculated in Figure 8 using the HadISST [*Rayner et al.*, 2003] and ERSSTv3b [*Smith et al.*, 2008] SST data sets, and the Delcroix ship-of-opportunity [*Delcroix et al.*, 2011] and ORA-S4 reanalysis [*Balmaseda et al.*, 2012] SSS data sets, which results in four combinations of data sets: HadISST/Delcroix, HadISST/ORA, ERSST/Delcroix, and ERSST/ORA. The magnitude of errors is estimated as the mean variance between the four pseudo-δ^{18}O time series (Table 5). In the fixed-slope case, the values are on the order of 0.001–0.01‰^{2} for most sites (or in standard

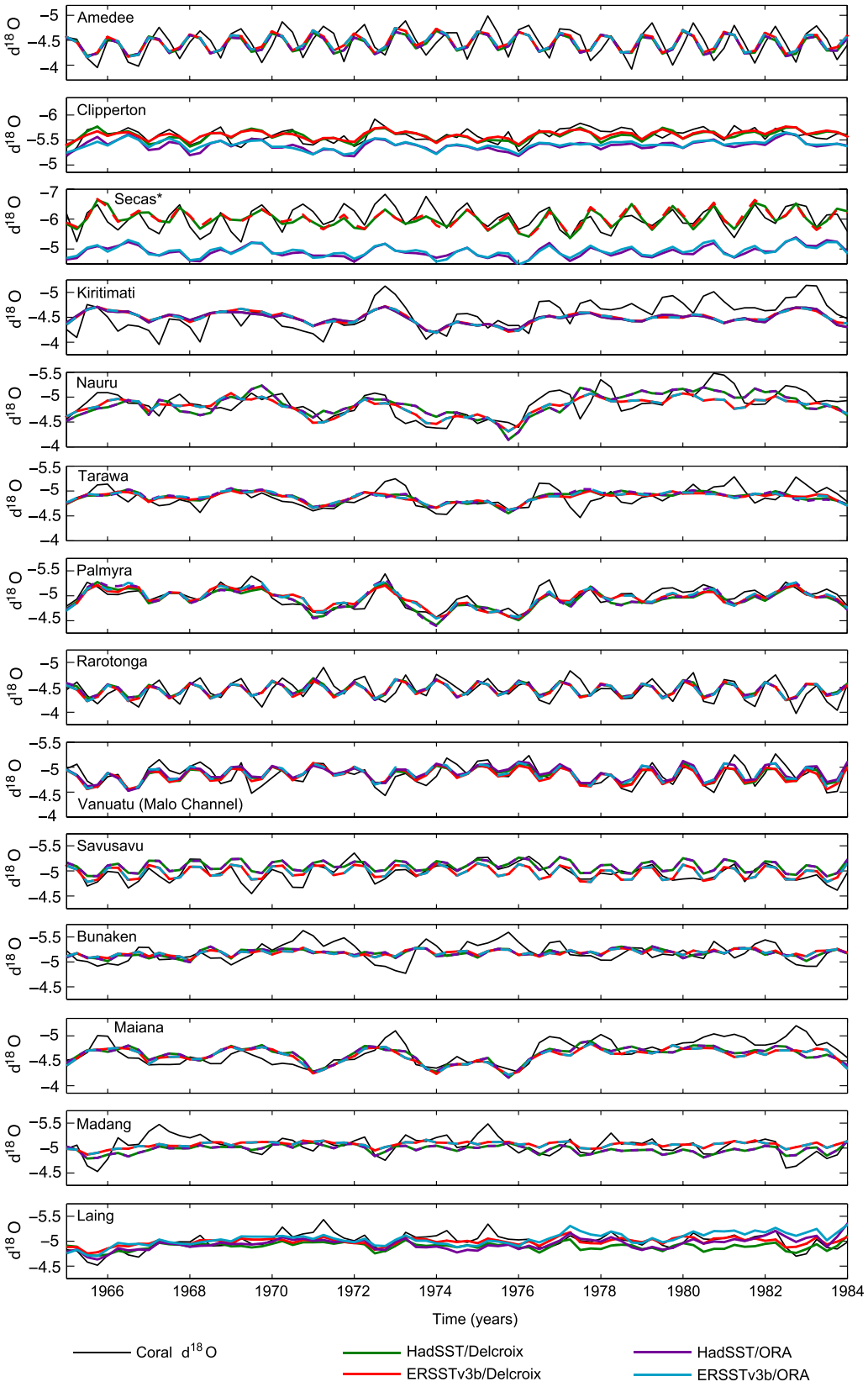

Figure 8. Fixed-slope monthly pseudo-δ^{18}O (‰) time series computed by applying Equation (1) to four different combinations of SST and SSS data products. All plots have the same *y* axis range (1.5‰), with the exception of Secas (indicated by the asterisk). HadISST/Delcroix SSS is shown in green, ERSSTv3b/Delcroix SSS in red, HadISST/ORA-S4 in purple, and ERSSTv3b/ORA-S4 in blue. Dashed lines were used where traces showed substantial overlap, to increase legibility.

Table 5. Mean Variances Between Pseudo-δ^{18}O Computed With All Possible Combinations of Data Products[a]

Site	Fit Variances	σ^2_{bf}	σ^2_{fs}
Bunaken	SST	0.020	0.020
Clipperton	SST, SSS	0.017	0.020
Kiritimati	SST	2.23×10^{-4}	0.0015
Laing	SST, SSS	0.0040	0.01
Madang	SST	0.0052	0.012
Maiana	SST, SSS	0.0016	0.0021
Nauru	SST, SSS	0.0021	0.0030
New Caledonia	SST, SSS	0.0021	0.0024
Palmyra	SST	0.0010	0.0024
Rarotonga	SST, SSS	0.0026	0.0037
Savusavu	SST, SSS	0.0028	0.01
Secas	SST, SSS	0.21	0.30
Tarawa	SST, SSS	4.84×10^{-4}	0.0021
Vanuatu (Malo Channel)	SST,SSS	0.0023	0.0037
Vanuatu (Sabine Bank)	SST,SSS	0.0020	0.0030

[a]Where a higher σ represents a larger scatter between fits to different instrumental products (less confidence in pseudo-δ^{18}O); σ^2_{bf} represents the mean variances between best fit pseudo-δ^{18}O time series while σ^2_{fs} for the fixed-slope pseudo-δ^{18}O. Units are ‰^{2}.

deviation units, 0.03–0.1‰), comparable to signal/age model errors but small compared with the errors in pseudo-δ^{18}O conversions.

[59] The time series of pseudo-δ^{18}O in Figure 8 suggest that the linear regression of δ^{18}O on SST and SSS does not provide a complete description of δ^{18}O variability. A more effective pseudo-δ^{18}O conversion method might be to look at other processes to include in the conversion relationship; this is investigated in the following section.

6. Improvements to Linear δ^{18}O Pseudoproxies

[60] A simple linear dependence of δ^{18}O on grid point SST and SSS seems to be insufficient for accurate ENSO amplitude estimation. One simple candidate improvement method is to account more accurately for the seasonal cycle, which may affect conditions near the proxy site by mechanisms other than variations in SST and SSS. Two good examples of locations which are strongly influenced by seasonality are Amedee Lighthouse in New Caledonia and Secas Island in Panama. At New Caledonia, the annual cycle in δ^{18}O is caused by seasonal SPCZ migrations [*Quinn et al.*, 1998], which create anomalies not only in SST but in δ^{18}O advection and rainfall as well [*Delcroix and Lenormand*, 1997]. In the case of Secas, *Linsley et al.* [1994] concluded that the coral δ^{18}O seasonal cycle is caused by changes to precipitation δ^{18}O due to seasonal migration of the ITCZ; in that study, the δ^{18}O value of precipitation was linearly related to coral δ^{18}O according to

$$\delta^{18}\mathrm{O}_{\mathrm{ppt}} = 47.99‰ + 8.72\delta^{18}\mathrm{O}_{\mathrm{coral}} \quad (6)$$

and seasonal variations dominated the signal far in excess of the SST influence.

[61] In the absence of more detailed δ^{18}O observations, the net seasonal cycle in δ^{18}O may be fit using sinusoids; the formulation of the fixed-slope pseudoproxy in (4) then becomes

$$\delta^{18}O = \beta_0 - \beta_T(\mathrm{SST}) + \beta_S(\mathrm{SSS}) + \beta_1 \sin(2\pi t) + \beta_2 \cos(2\pi t) \quad (7)$$

where t is the date expressed in years and both the sine and cosine terms are retained to allow the phase of the δ^{18}O seasonal cycle to vary. This approach is numerically equivalent to fitting a sinusoidal function to the residuals from (4); if the resulting fit is able to describe a larger proportion of the variance, this is an indication that there is a seasonally varying signal in δ^{18}O which is not described by SST and SSS alone, such as advective/source region effects.

[62] The "fixed-slope-seasonal" (FSS) pseudoproxy relationship in (7) was fit to all coral time series; 9 out of 15 sites show a statistically significant contribution from the seasonal cycle, as indicated by the bold entries in Table 6. As expected, Secas and New Caledonia are among those sites that are well fitted by (7), and the resulting FSS fits for these sites are shown in Figure 9. Notably, even locations where δ^{18}O does not show a visually obvious sinusoidal pattern (Kiritimati, Palmyra, Laing and Madang) see improvements to pseudo-δ^{18}O. This is consistent with the

Table 6. Errors in Pseudo-δ^{18}O Variance[a]

Site	σ^2 δ^{18}O (‰^{2})	FS + Age	FSS + Age
Bunaken	0.030	0.015 (49)	0.014 (48)
Clipperton	0.016	0.011 (66)	0.010 (66)
Kiritimati	0.077	0.029 (38)	0.027 (35)
Laing	0.026	0.015 (58)	0.014 (57)
Madang	0.031	0.016 (50)	0.015 (49)
Maiana	0.060	0.022 (36)	0.021 (36)
Nauru	0.070	0.026 (37)	0.024 (35)
New Caledonia	0.065	0.032 (50)	0.028 (44)
Palmyra	0.036	0.014 (39)	0.014 (39)
Rarotonga	0.037	0.028 (75)	0.020 (55)
Savusavu	0.044	0.022 (49)	0.019 (44)
Secas	0.13	0.047 (37)	0.042 (33)
Tarawa	0.036	0.021 (58)	0.020 (55)
Vanuatu (Malo Channel)	0.048	0.021 (44)	0.017 (36)
Vanuatu (Sabine Bank)	0.039	0.020 (50)	0.019 (48)

[a]The first column shows the total variance in the time series over 1958–1985, and errors are then listed in ‰^{2} (and in percent) for the total error (residual plus age) in the fixed-slope pseudoproxy (FS + Age) and the total error for the fixed-slope pseudoproxy including the seasonal cycle (FSS + Age). Both the FS + Age and FSS + Age columns represent 1σ uncertainties on the δ^{18}O variance in the first column. Entries in bold indicate sites where inclusion of the seasonal cycle term results in a significant reduction in δ^{18}O variance error. As in Table 3, the signal/age model error calculated for individual sites is applied to those sites, and for all others, the mean of the site-specific calculations is used.

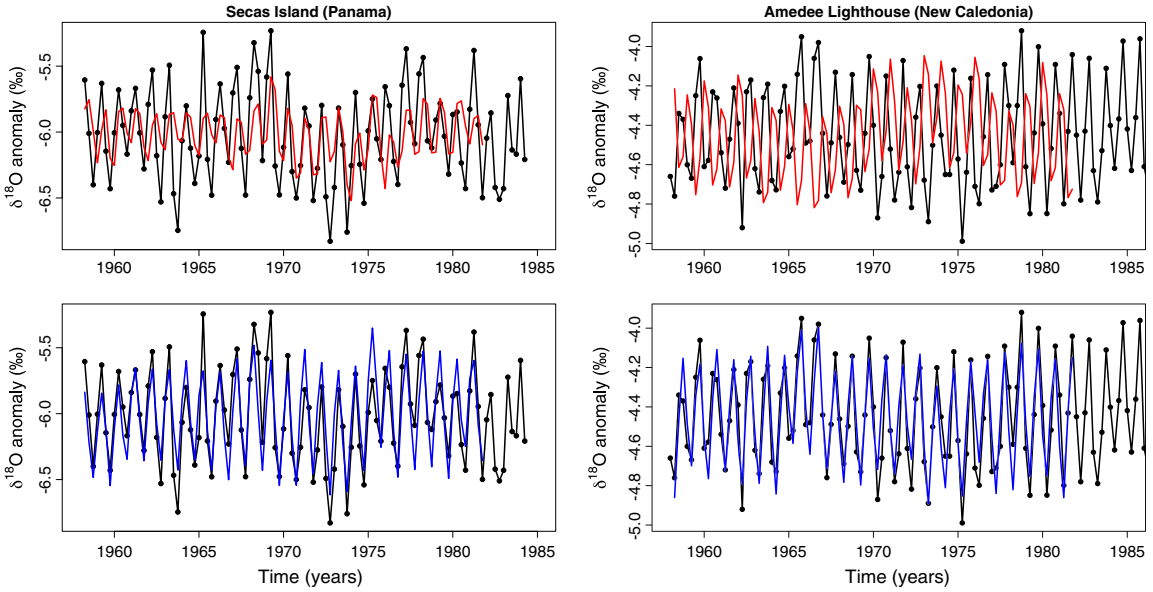

Figure 9. Pseudo-δ^{18}O for (left column) Secas Island, Panama, and (right column) Amedee Lighthouse, New Caledonia. (top row) Fixed-slope pseudo-δ^{18}O calculated using ERSSTv3b and ORA-S4 (red) compared with the original coral δ^{18}O record (black). (bottom row) Fixed-slope pseudo-δ^{18}O, with the addition of sine and cosine terms for the seasonal cycle (equation (7); blue), compared to the original coral δ^{18}O (black).

finding of *McGregor et al.* [2011] that the annual cycle accounts for 15% of the modern Kiritimati δ^{18}O variance, partly related to the westward propagation of SST anomalies near the equator.

[63] The seasonal fits included here are a simple improvement to pseudoproxy conversions and indeed are a natural extension of the *Thompson et al.* [2011] pseudoproxies which used the same SST and SSS dependencies. However, it is important to note that although (7) allows *improvements* in δ^{18}O variance estimates, the errors still remain at 30% or more of the input value; future work will be required to further improve model/proxy conversion.

7. Discussion and Future Recommendations

[64] The present study is aimed at improving quantitative model ENSO validation against coral δ^{18} records through the use of empirical "pseudoproxy/forward model" conversions. Although such conversions are less mathematically sophisticated than multiproxy statistical methods [*Mann et al.*, 2009; *Wilson et al.*, 2010], there are nonetheless advantages, namely, the relaxation of the assumption of large-scale stationarity and of the requirement for high data density. The character of ENSO is known to change from event to event [*Ashok et al.*, 2007], affecting the strength of the covariance between ENSO and any given proxy location; empirical conversions assume stationarity only in the sensitivity of the proxy to local climate, a less restrictive assumption. Empirical conversions also have the potential to allow accurate ENSO reconstruction given a far smaller sample size than field reconstructions, which typically require a minimum of several dozen records [*Mann et al.*, 2009]—far beyond what is currently achievable for subannually resolved, synchronous fossil corals. Better local climate/δ^{18}O conversions should thus allow existing coral records to provide much more useful information.

[65] The ENSO estimates produced by linear approximations such as (4) have such large errors that they are consistent with pseudo-δ^{18}O values derived from climate model output (not pictured). In this situation, it becomes nearly impossible to use coral δ^{18}O measurements to motivate specific improvements to model ENSO behavior, or alternately to use simulations of past climates to examine the potential causes for shifts in δ^{18}O signals. Through an improved understanding of the mechanisms generating coral δ^{18}O anomalies, it will become possible to construct more detailed dynamical ENSO diagnostics, and thus to improve the utility of both climate models and fossil δ^{18}O records.

[66] Deriving improved forward models for δ^{18}O is complex. The true seawater δ^{18}O will be affected by changes to advection past the proxy location, by changes to water mass properties, by the relative amounts of precipitation and evaporation, and by the δ^{18}O values within local precipitation (itself a function of the source region, atmospheric water vapor transport, and other fractionation processes). These effects may sometimes be difficult to detect below a given "threshold," as observed by *McGregor et al.* [2011] for the precipitative influence on seawater δ^{18}O at Kiritimati; this may contribute to errors in the linear pseudoproxies of *Brown et al.* [2008], *Thompson et al.* [2011], and *Phipps et al.* [2013].

[67] The most accurate description of δ^{18}O based on local conditions is the δ^{18}O budget:

$$\frac{\partial(\mathrm{O}_{sw})}{\partial t} + \nabla \cdot (\vec{v}\mathrm{O}_{sw}) = \Phi_P \mathrm{O}_P - \Phi_E \mathrm{O}_E \tag{8}$$

where Φ_P and Φ_E are the fluxes of precipitation and evaporation, $\nabla \cdot (\vec{v}O_{sw})$ is the advection of seawater δ^{18}O, and O_{sw}, O_P, and O_E are the δ^{18}O values for seawater, precipitation, and evaporation, respectively. The complexity and coupled nature of the processes involved quickly lead to this approach becoming indistinguishable from the physics in an isotope-enabled GCM. Yet an approach like (8) is ultimately the only way to correctly account for the relative importance of various influences on δ^{18}O, since many of these effects may dominate over SST and SSS influences. Indeed, a preliminary diagnosis of (8) using ORA-S4 reanalysis data shows qualitative similarities between changes to coral δ^{18}O and upper layer ocean advection at a variety of sites (not pictured). This highlights the potential of GCMs to provide valuable physical insights into fossil coral δ^{18}O records, as noted recently by *Russon et al.* [2013], and should serve as motivation for improving the state of coral/model comparison techniques.

8. Conclusions

[68] This work has assessed the errors associated with ENSO reconstruction from coral δ^{18}O, using modern corals from 15 sites covering the period 1958–1985. The δ^{18}O observational error at a given site (the "signal/age model error") is found to be 0.12–0.14‰ using records from three locations: Kiritimati Island [*Evans et al.*, 1998b; *Woodroffe and Gagan*, 2000; *Woodroffe et al.*, 2003; *Nurhati et al.*, 2009; *McGregor et al.*, 2011], Amedee Lighthouse in New Caledonia [*Stephans et al.*, 2004], and Rarotonga [*Linsley et al.*, 2006]. Such intercoral offsets lead to typical variance errors of roughly 8–25%. Although substantial, signal/age model errors do not preclude the accurate estimation of the PC1 power spectrum of δ^{18}O. Errors from dating uncertainties of ±5 to 10 years are also fairly small. The required sample size for reconstructing the majority of ENSO-related variance seems to be roughly five to seven sites, based on an analysis of δ^{18}O PC1. However, the choice of sampling location critically affects the character of δ^{18}O PC1 and PC2. ENSO variability with largest loading in the eastern Pacific is detected as both PC1 and PC2 by sites in the cold tongue, warm pool, and SPCZ, while a pattern resembling the Modoki El Niño appears in PC2 when cores from the warm pool and SPCZ regions are combined. Regardless of the location of the ENSO center of action, a minimum of two to four corals seems to be required.

[69] A Monte Carlo error analysis on linear pseudoproxies of the form used by *Thompson et al.* [2011] shows that the major obstacle to quantitative ENSO amplitude estimation using δ^{18}O is its conversion to climate variables. Instrumental/grid point uncertainties in observational SST and SSS products lead to a variance of roughly 0.001–0.01‰^{2} between pseudo-δ^{18}O calculated with different data products, an error of the same order of magnitude as signal/age model uncertainties. The offsets between pseudo-δ^{18}O time series seem to be largest at sites where the temperature influence does not dominate, indicating that a detailed understanding of controls on seawater δ^{18}O will be required to improve pseudo-δ^{18}O accuracy. Fit residuals, both using regression slopes specified from prior knowledge of the δ^{18}O relationships with SST and SSS and from site-specific least squares estimation, result in errors of 37–75% of the original δ^{18}O variance. These errors are so large that they dominate even the covarying modes between locations, as demonstrated by calculating the first PC using multiple linear pseudo-δ^{18}O time series biased according to the appropriate error distributions.

[70] The importance of correctly representing changes to seawater δ^{18}O (or local-scale processes) is confirmed by including a sinusoidal component with a period of 1 year in the fixed-slope linear pseudoproxy conversion. This is intended to account for the combined influence of advective and atmospheric source effects on the seasonal cycle of δ^{18}O and results in a statistically significant improvement in conversion performance at 9 of 15 sites. However, errors remain at or above 30% for all locations.

[71] To improve δ^{18}O-based ENSO reconstructions, we recommend improving environmental monitoring at coral sites with a focus on SST, SSS, ocean velocities, evaporation/relative humidity, seawater δ^{18}O, and δ^{18}O of precipitation. By doing so, the contribution of all of these influences to coral δ^{18}O variations may be more accurately quantified, allowing more accurate model/proxy conversions to better illustrate the dynamical linkages between ENSO characteristics and δ^{18}O variations near the proxy site.

[72] **Acknowledgments.** S.S. was supported by a CIRES Innovative Research Project grant for travel in Australia. This work is supported by Australian Research Council Discovery Project grant DP1092945. H.V.M. is supported by an AINSE Research Fellowship. C. Charles, A. Timmermann and A. Tudhope are gratefully acknowledged for helpful discussions which greatly improved the manuscript.

References

Alibert, C., and L. Kinsley (2008), A 170-year Sr/Ca and Ba/Ca coral record from the western Pacific warm pool: 1. What can we learn from an unusual coral record?, *J. Geophys. Res.*, *113*, C04008, doi:10.1029/2006JC003979.

Ashok, K., S. Behera, A. Rao, H. Weng, and T. Yamagata (2007), El Niño Modoki and its teleconnection, *J. Geophys. Res.*, *112*, C11007, doi:10.1029/2006JC003798.

Bagnato, S., B. Linsley, S. Howe, G. Wellington, and J. Salinger (2004), Evaluating the use of the massive coral Diploastrea heliopora for paleoclimate reconstruction, *Paleoceanography*, *19*, PA1032, doi:10.1029/2003PA000935.

Balmaseda, M., K. Mogensen, and A. Weaver (2012), Evaluation of the ECMWF ocean reanalysis system ORAS4, *Q. J. R. Meteorol. Soc.*, *139*, 1132–1161, doi:10.1002/qj.2063.

Brown, J., A. W. Tudhope, M. Collins, and H. V. McGregor (2008), Mid-Holocene ENSO: Issues in quantitatve model-proxy data comparisons, *Paleoceanography*, *23*, PA3202, doi:10.1029/2007PA001512.

Cahyarini, S. Y., M. Pfeiffer, O. Timm, W.-C. Dullo, and D. G. Schonberg (2008), Reconstructing seawater δ^{18}O from paired coral δ^{18}O and Sr/Ca ratios: Methods, error analyses and problems, with examples from Tahiti (French Polynesia) and Timor (Indonesia), *Geochim. Cosmochim. Acta*, *72*, 2841–2853.

Carré, M., J. Sachs, J. M. Wallace, and C. Favier (2012), Exploring errors in paleoclimate proxy reconstructions using Monte Carlo simulations: Paleotemperature from mollusk and coral geochemistry, *Clim. Past*, *8*, 433–450.

Charles, C., K. Cobb, M. Moore, and R. Fairbanks (2003), Monsoon-tropical ocean interaction in a network of coral records spanning the 20th century, *Mar. Geol.*, *201*, 207–222.

Charles, C., D. Hunter, and R. Fairbanks (1997), Interaction between the ENSO and the Asian Monsoon in a coral record of tropical climate, *Science*, *277*, 925–927.

Cheng, H., et al. (2013), Improvements in 230Th dating, 230Th and 234U half-life values, and UTh isotopic measurements by multi-collector inductively coupled plasma mass spectrometry, *Earth Planet. Sci. Lett.*, *371*, 82–91.

Cobb, K., C. Charles, H. Cheng, and R. Edwards (2003), El Niño/Southern Oscillation and tropical Pacific climate during the last millennium, *Nature*, *424*, 271–276.

Cobb, K., C. Charles, and D. Hunter (2001), A central tropical Pacic coral demonstrates Pacic, Indian, and Atlantic decadal climate connections, *Geophys. Res. Lett.*, *28*, 2209–2212.

Cole, J. E., R. G. Fairbanks, and G. T. Shen (1993), Recent variability in the Southern Oscillation: Isotopic results from a Tarawa Atoll Coral, *Science*, *260*, 1790–1793.

Collins, M., et al. (2010), The impact of global warming on the tropical Pacific Ocean and El Niño, *Nat. Geosci.*, *3*, 391–397, doi:10.1038/NGEO868.

Correge, T. (2006), Sea surface temperature and salinity reconstruction from coral geochemical tracers, *Palaeogeogr. Palaeoclimatol. Palaeoecol.*, *232*, 408–428.

D'Arrigo, R., R. Wilson, J. Palmer, P. Krusic, A. Curtis, J. Sakulich, S. Bijaksana, S. Zulaikah, L. O. Ngkoimani, and A. Tudhope (2006), The reconstructed Indonesian warm pool sea surface temperatures from tree rings and corals: Linkages to Asian monsoon drought and El Niño-Southern Oscillation, *Paleoceanography*, *21*, PA3005, doi:10.1029/2005PA001256.

Delcroix, T., G. Alory, S. Cravatte, T. Correge, and M. J. McPhaden (2011), A gridded sea surface salinity data set for the tropical Pacific with sample applications (1950-2008), *Deep Sea Res.*, *58*, 38–48.

Delcroix, T., and O. Lenormand (1997), ENSO signals in the vicinity of New Caledonia, South-Western Tropical Pacific, *Oceanol. Acta*, *20*, 481–491.

DeLong, K., T. M. Quinn, F. W. Taylor, K. Lin, and C.-C. Shen (2012), Sea surface temperature variability in the southwest tropical Pacific since AD 1649, *Nat. Clim. Change*, *2*, 799–804.

DeLong, K., T. M. Quinn, F. W. Taylor, C.-C. Shen, and K. Lin (2013), Improving coral-base paleoclimate reconstructions by replicating 350 years of coral Sr/Ca variations, *Palaeogeogr. Palaeoclimatol. Palaeoecol.*, *373*, 6–24.

DeLong, K. L., T. M. Quinn, and F. W. Taylor (2007), Reconstructing twentieth-century sea surface temperature variability in the southwest Pacific: A replication study using multiple coral Sr/Ca records from New Caledonia, *Paleoceanography*, *22*, PA4212, doi:10.1029/2007PA001444.

Deser, C., A. S. Phillips, and M. A. Alexander (2010), Twentieth century tropical sea surface temperature trends revisited, *Geophys. Res. Lett.*, *37*, L10701, doi:10.1029/2010GL043321.

Dunbar, R., G. Wellington, M. Colgan, and P. Glynn (1994), Eastern Pacific sea surface temperature since 1600 AD: The δ^{18}O record of climate variability in Galapagos corals, *Paleoceanography*, *9*(2), 291–315.

Emile-Geay, J., K. Cobb, M. Mann, and A. T. Wittenberg (2013), Estimating tropical pacific SST variability over the past millennium. Part 2: Reconstructions and Uncertainties, *J. Clim.*, *26*, 2329–2352.

Epstein, S., R. Buchsbaum, H. A. Lowenstam, and H. C. Urey (1953), Revised carbonate/water isotopic temperature scale, *Geol. Soc. Am. Bull.*, *64*(11), 1315–1326, doi:10.1130/0016-7606(1953)64[1315:RCITS]2.0.CO;2.

Evans, M. N., R. G. Fairbanks, and J. L. Rubenstone (1998a), *Kiritimati Coral Isotope Data. IGBP PAGES/World Data Center-A for Paleoclimatology Data Contribution Series, 1998–035*, NOAA/NGDC Paleoclimatology Program, Boulder, CO, USA.

Evans, M. N., R. G. Fairbanks, and J. L. Rubenstone (1999), The thermal oceanographic signal of El Niño reconstructed from a Kiritimati Island coral, *J. Geophys. Res.*, *104*(C6), 13,409–13,421.

Evans, M. N., A. Kaplan, and M. A. Cane (1998b), Optimal sites for coral-based reconstructions of global sea surface temperature, *Paleoceanography*, *13*(5), 502–516.

Evans, M. N., A. Kaplan, and M. A. Cane (2000), Intercomparison of coral oxygen isotope data and historical sea surface temperature (SST): Potential for coral-based SST field reconstructions, *Paleoceanography*, *15*(5), 551–562.

Evans, M. N., A. Kaplan, and M. A. Cane (2002), Pacific sea surface temperature field reconstruction from coral δ^{18}O data using reduced space objective analysis, *Paleoceanography*, *17*(1), 1007, doi:10.1029/2000PA000590.

Fairbanks, R., M. Evans, J. Rubenstone, R. Mortlock, K. Broad, M. Moore, and C. Charles (1997), Evaluating climate indices and their geochemical proxies measured in corals, *Coral Reefs*, *16*, S93–S100.

Felis, T., J. Pätzold, Y. Loya, M. Fine, A. H. Nawar, and G. Wefer (2000), A coral oxygen isotope record from the northern Red Sea documenting NAO, ENSO and North Pacific teleconnections on Middle East climate variability since the year 1750, *Paleoceanography*, *15*(6), 679–694.

Gagan, M., and N. Abram (2011), Stable isotopes and trace elements, in *Encyclopedia of Modern Coral Reefs: Structure, Form and Process*, edited by D. Hopley, pp. 1034–1043, Springer, Heidelberg, Germany.

Gagan, M., G. Dunbar, and A. Suzuki (2012), The effect of skeletal mass accumulation in *Porites* on coral Sr/Ca and δ^{18}O paleothermometry, *Paleoceanography*, *27*, PA1203, doi:10.1029/2011PA002215.

Gagan, M. K., L. D. Ayliffe, D. Hopley, J. A. Cale, G. E. Mortimer, J. Chappell, M. T. McCulloch, and M. J. Head (1998), Temperature and surface-ocean water balance of the mid-holocene tropical western pacific, *Science*, *279*, 1014–1018.

Gorman, M. K., T. M. Quinn, F. W. Taylor, J. W. Partin, G. Cabioch, J. A. Austin Jr., B. Pelletier, V. Ballu, C. Maes, and S. Saustrup (2012), A coral-based reconstruction of sea surface salinity at Sabine Bank, Vanuatu from 1842 to 2007 CE, *Paleoceanography*, *27*, PA3226, doi:10.1029/2012PA002302.

Grottoli, A., and C. Eakin (2007), A review of modern coral δ^{18}18O and Δ^{14}C proxy records, *Earth Sci. Rev.*, *81*, 67–91.

Guilderson, T. P., and D. P. Schrag (1999), Reliability of coral iso- tope records from the Western Pacic warm pool: A compar- ison using age-optimized records, *Paleoceanography*, *14*, 457–464.

Guilyardi, E., A. Wittenberg, A. Fedorov, M. Collins, C. Wang, A. Capotondi, G. Jan van Oldenborgh, and T. Stockdale (2009), Understanding El Niño in ocean-atmosphere general circulation models: Progress and challenges, *Bull. Am. Meteorol. Soc.*, *90*, 325–340.

Hereid, K. A., T. M. Quinn, and Y. M. Okumura (2013), Assessing spatial variability in El Niño Southern Oscillation event detection skill using coral geochemistry, *Paleoceanography*, *18*, 14–23.

Horel, J. D., and J. M. Wallace (1981), Planetary scale atmospheric phenomena associated with the Southern Oscillation, *Mon. Weather Rev.*, *109*, 813–829.

Kilbourne, K., T. Quinn, F. Taylor, T. Delcroix, and Y. Gouriou (2004), El Nino-Southern Oscillation-related salinity variations recorded in the skeletal geochemistry of a Porites coral from Espiritu Santo, Vanuatu, *Paleoceanography*, *19*, PA4002, doi:10.1029/2004PA001033.

LaVigne, M., I. S. Nurhati, K. M. Cobb, H. V. McGregor, D. Sinclair, and R. M. Sherrell (2013), Systematic ENSO-driven nutrient variability recorded by central equatorial Pacific corals, *Geophys. Res. Lett.*, *40*, 3956–3961, doi:10.1002/grl.50765.

LeGrande, A. N., and G. A. Schmidt (2006), Global gridded data set of the oxygen isotopic composition in seawater, *Geophys. Res. Lett.*, *33*, L12604, doi:10.1029/2006GL026011.

Linsley, B., A. Kaplan, Y. Gouriou, J. Salinger, P. deMenocal, G. Wellington, and S. Howe (2006), Tracking the extent of the South Pacific Convergence Zone since the early 1600s, *Geochem. Geophys. Geosyst.*, *7*, Q05003, doi:10.1029/2005GC001115.

Linsley, B. K., R. B. Dunbar, G. M. Wellington, and D. A. Mucciarone (1994), A coral-based reconstruction of Intertropical Convergence Zone variability over Central America since 1707, *J. Geophys. Res.*, *99*, 9977–9994.

Linsley, B. K., R. G. Messier, and R. B. Dunbar (1999), Assessing between-colony oxygen isotope variability in the coral *Porites lobata* at Clipperton Atoll, *Coral Reefs*, *18*, 13–27.

Lough, J. (2004), A strategy to improve the contribution of coral data to high-resolution paleoclimatology, *Palaeogeogr. Palaeoclimatol. Palaeoecol.*, *204*, 115–143.

Lough, J. M. (2010), Climate records from corals, *WIREs Clim. Change*, *1*, 318–331, doi:10.1002/wcc.39.

Mann, M. E., Z. Zhang, M. K. Hughes, R. S. Bradley, S. K. Miller, S. Rutherford, and F. Ni (2008), Proxy-based reconstructions of hemispheric and global surface temperature variations over the past two millennia, *Proc. Natl. Acad. Sci. USA*, *105*, 13,253–13,257.

Mann, M. E., et al. (2009), Global signatures and dynamical origins of the little ice age and medieval climate anomaly, *Science*, *326*, 1256–1260.

McGregor, H., and N. Abram (2008), Images of diagenetic textures in Porites corals from Papua New Guinea and Indonesia, *Geochem. Geophys. Geosyt.*, *9*, Q10013, doi:10.1029/2008GC002093.

McGregor, H. V., M. J. Fischer, M. K. Gagan, D. Fink, S. J. Phipps, H. Wong, and C. D. Woodroffe (2013), A weak El Niño-Southern Oscillation with delayed seasonal growth around 4,300 years ago, *Nat. Geosci.*, doi:10.1038/ngeo1936.

McGregor, H. V., M. J. Fischer, M. K. Gagan, D. Fink, and C. D. Woodroffe (2011), Environmental control of the oxygen isotope composition of Porites coral microatolls, *Geochim. Cosmochim. Acta*, *75*, 3930–3944.

McGregor, H. V., and M. K. Gagan (2004), Western Pacific coral δ^{18}O records of anomalous Holocene variability in the El Niño-Southern Oscillation, *Geophys. Res. Lett.*, *31*, L11204, doi:10.1029/2004GL019972.

Nurhati, I., K. Cobb, C. Charles, and R. Dunbar (2009), Late 20th century warming and freshening in the central tropical Pacific, *Geophys. Res. Lett.*, *36*, L21606, doi:10.1029/2009GL040270.

Nurhati, I. S., K. M. Cobb, and E. Di Lorenzo (2011), Decadal-Scale SST and salinity variations in the central tropical pacific: Signatures of natural and anthropogenic climate change, *J. Clim.*, *24*, 3294–3308.

Phipps, S. J., H. V. McGregor, J. Gergis, A. J. E. Gallant, R. Neukom, S. Stevenson, D. Ackerley, J. R. Brown, M. J. Fischer, and T. D. Van Ommen (2013), Paleoclimate data-model comparison and the role of climate forcings over the past 1500 years, *J. Clim.*, *26*, 6915–6936, doi:10.1175/JCLI-D-12-00108.1.

Quinn, T. M., T. J. Crowley, F. W. Taylor, C. Henin, P. Joannot, and Y. Join (1998), A multicentury stable isotope record from a New Caledonia coral: Interannual and decadal SST variability in the southwest Pacific since 1657, *Paleoceanography*, *13*, 412–426.

Ray, S., and B. S. Giese (2012), Historical changes in El Niño and La Niña characteristics in an ocean reanalysis, *J. Geophys. Res.*, *117*, C11007, doi:10.1029/2012JC008031.

Rayner, N. A., D. E. Parker, E. B. Horton, C. K. Folland, L. V. Alexander, D. P. Rowell, E. C. Kent, and A. Kaplan (2003), Global analyses of sea surface temperature, sea ice, and night marine air temperature since the late nineteenth century, *J. Geophys. Res.*, *108*(D14), 4407, doi:10.1029/2002JD002670.

Ropelewski, C. F., and M. S. Halpert (1986), North American precipitation and temperature patterns associated with the El Niño/Southern Oscillation, *Mon. Weather Rev.*, *114*, 2352–2362.

Russon, T., A. W. Tudhope, G. C. Hegerl, M. Collins, and J. Tindall (2013), Inter-annual tropical Pacific climate variability in an isotope-enabled CGCM: Implications for interpreting coral stable oxygen isotope records of ENSO, *Clim. Past*, *9*, 1543–1557.

Shen, C.-C., et al. (2008), Variation of initial $^{230}Th/^{232}Th$ and limits of high precision UTh dating of shallow-water corals, *Geochim. Cosmochim. Acta*, *72*, 4201–4223.

Singh, A., T. Delcroix, and S. Cravatte (2011), Contrasting the flavors of El Niño-Southern Oscillation using sea surface salinity observations, *J. Geophys. Res.*, *116*, C06016, doi:10.1029/2010JC006862.

Smerdon, J. (2012), Climate models as a test bed for climate reconstruction methods: Pseudoproxy experiments, *WIREs Clim. Change*, *3*, 63–77, doi:10.1002/wcc.149.

Smith, T., R. W. Reynolds, T. C. Peterson, and J. Lawrimore (2008), Improvements to NOAA's historical merged land-ocean surface temperature analysis (1880-2006), *J. Clim.*, *21*, 2283–2296.

Solomon, A., and M. Newman (2012), Reconciling disparate twentieth-century Indo-Pacific ocean temperature trends in the instrumental record, *Nat. Clim. Change*, *2*, 691–699, doi:10.1038/nclimate1591.

Stephans, C. L., T. M. Quinn, F. W. Taylor, and T. Correge (2004), Assessing the reproducibility of coral-based climate records, *Geophys. Res. Lett.*, *31*, L18210, doi:10.1029/2004GL020343.

Stevenson, S., B. Fox-Kemper, M. Jochum, R. Neale, C. Deser, and G. Meehl (2012), Will there be a significant change to El Niño in the 21st century?, *J. Clim.*, *25*, 2129–2145, doi:10.1175/JCLI-D-11-00252.1.

Stevenson, S., B. Fox-Kemper, M. Jochum, B. Rajagopalan, and S. Yeager (2010), Model ENSO validation using wavelet probability analysis, *J. Clim.*, *23*, 5540–5547.

Thompson, D. M., T. R. Ault, M. N. Evans, J. E. Cole, and J. Emile-Geay (2011), Comparison of observed and simulated tropical climate trends using a forward model of coral $\delta^{18}O$, *Geophys. Res. Lett.*, *38*, L14706, doi:10.1029/2011GL048224.

Tokinaga, H., S.-P. Xie, A. Timmermann, S. McGregor, T. Ogata, H. Kubota, and Y. Okumura (2012), Regional patterns of tropical Indo-Pacific climate change: Evidence of the walker circulation weakening, *J. Clim.*, *25*, 1689–1710, doi:10.1175/JCLI-D-11-00263.1.

Tudhope, A. W., C. P. Chilcott, M. T. McCulloch, E. R. Cook, J. Chappell, R. M. Ellam, D. W. Lea, J. M. Lough, and G. B. Shimmield (2001), Variability in the El Niño/Southern Oscillation through a glacial-interglacial cycle, *Science*, *291*, 1511–1517.

Urban, F., J. Cole, and J. Overpeck (2000), Influence of mean climate change on climate variability from a 155- year tropical Pacic coral record, *Nature*, *407*, 989–993.

Venables, W. N., and B. D. Ripley (2002), *Modern Applied Statistics with S,* 4th ed., Springer, New York.

Wilson, R., E. Cook, R. D'Arrigo, N. Riedwyl, M. N. Evans, A. Tudhope, and R. Allan (2010), Reconstructing ENSO: The influence of method, proxy data, climate forcing and teleconnections, *J. Quaternary Sci.*, *25*(1), 62–78.

Wittenberg, A. T. (2009), Are historical records sufficient to constrain ENSO simulations?, *Geophys. Res. Lett.*, *36*, L12702, doi:10.1029/2009GL038710.

Woodroffe, C. D., M. R. Beech, and M. K. Gagan (2003), Mid-late Holocene El Niño variability in the equatorial Pacific from coral microatolls, *Geophys. Res. Lett.*, *30*, 1358, doi:10.1029/2002GL015868.

Woodroffe, C. D., and M. K. Gagan (2000), Coral microatolls from the central Pacific record late Holocene El Niño, *Geophys. Res. Lett.*, *27*, 1511–1514.

Zhao, J.-x., K.-f. Yu, and Y.-x. Feng (2009), High-precision ^{238}U-^{234}U-^{230}Th dissequilibrium dating of the recent past: A review, *Quat. Geochronol.*, *4*, 423–433.